

1 **Assessing the influence of water sampling strategy on the performance of tracer-**
2 **aided hydrological modeling in a mountainous basin on the Tibetan Plateau**

3 Yi Nan¹, Zhihua He², Fuqiang Tian¹, Zhongwang Wei³, Lide Tian⁴

4 ¹ Department of Hydraulic Engineering, State Key Laboratory of Hydrosience and Engineering,
5 Tsinghua University, Beijing, China

6 ² Center for Hydrology, University of Saskatchewan, Saskatchewan, Canada

7 ³ Guangdong Province Key Laboratory for Climate Change and Natural Disaster Studies, School of
8 Atmospheric Sciences, Sun Yat-sen University, Guangzhou, Guangdong, China

9 ⁴ Institute of International Rivers and Eco-security, Yunnan University, Kunming, China

10 ***Corresponding to:*** Fuqiang Tian

11 Email: tianfq@tsinghua.edu.cn

12

13 **Abstract**

14 Tracer-aided hydrological models integrating water isotope module into the simulation of
15 runoff generation are useful tools to reduce uncertainty of hydrological modeling in cold basins
16 that are featured by complex runoff processes and multiple runoff components. However, there
17 is little guidance on the strategy of field water sampling for isotope analysis to run tracer-aided
18 hydrological models, which is especially important for large mountainous basins on the Tibetan
19 Plateau (TP) where field water sampling work is highly costly. This study conducted a set of
20 numerical experiments based on the THREW-T ([Tsinghua Representative Elementary](#)
21 [Watershed - Tracer-aided version](#)) model to evaluate the reliance of the tracer-aided modeling
22 performance on the availability of site measurements of water isotope in the Yarlung Tsangpo
23 River (YTR) basin on the TP. Data conditions considered in the numerical experiments included
24 the availability of glacier meltwater isotope measurement, quantity of site measurements of
25 precipitation isotope, and the variable collecting strategies for stream water sample. Our results
26 suggested that: (1) In high-mountain basins where glacier meltwater samples for isotope
27 analysis are not available, estimating glacier meltwater isotope by an offset parameter from the
28 precipitation isotope is a feasible way to force the tracer-aided hydrological model. Using a set
29 of glacier meltwater $\delta^{18}\text{O}$ that were 2‰~9‰ lower than the mean precipitation $\delta^{18}\text{O}$ resulted in
30 only small changes in the model performance and the quantifications of contributions of runoff
31 components (CRCs, smaller than 5%) to streamflow in the YTR basin; (2) [S](#)strategy of field
32 sampling for site precipitation to correct the global gridded isotope product of isoGSM for
33 model forcing should be carefully designed. Collecting precipitation samples at sites falling in
34 the same altitude tends to be worse at representing the ground pattern of precipitation $\delta^{18}\text{O}$ over
35 the basin than collecting precipitation samples from sites in a range of altitudes; (3) Collecting
36 weekly stream water samples at multiple sites in the wet and warm seasons is the optimal
37 strategy for calibrating and evaluating a tracer-aided hydrological model in the YTR basin. It is
38 highly recommended to increase the number of stream water sampling sites rather than
39 spending resource on extensive sampling of stream water at a sole site for multiple years. These
40 results provide important implications for collecting site measurements of water isotope for
41 running tracer-aided hydrological models to improve quantifications of CRCs in the [large](#) high-
42 mountain basins.

43

44 1. Introduction

45 Catchments located in mountainous regions generally provide important water resources
46 for downstream regions (Viviroli et al., 2003). As typical mountainous cryosphere, [the Tibetan](#)
47 [Plateau \(TP\)](#) is the source region for several large rivers in Asia, and has been called as [a](#) ‘water
48 tower’ because of its importance for downstream livelihoods and agricultural irrigations
49 (Schaner et al., 2012). Dominant characteristic of mountainous catchments on TP is the
50 multiphase of water sources that generate runoff and the consequently complex hydrological
51 processes, highlighting the importance of accurately quantifying the contributions of runoff
52 components (CRCs) to streamflow for better understandings ~~of~~ the runoff dynamics under
53 changing climate. This task is difficult due to the complex hydrological processes being
54 insufficiently represented by typical hydrological models, leading to large uncertainty of
55 hydrological simulations (He et al., 2018). Due to the strong inter-compensation of runoff
56 processes induced by different water sources and runoff pathways (Duethmann et al., 2015),
57 uncertainties of the modeled CRCs in mountainous basins on the TP are rather high. Utilizing
58 more datasets to evaluate the model performance is a feasible way to constrain modeling
59 uncertainty and improve quantifications of CRCs in cold regions (Chen et al., 2017).

60 Tracer-aided hydrological models integrating environmental tracer (e.g., stable oxygen
61 isotope, ^{18}O) modules into runoff generation processes have proved helpful for parameter
62 calibration, model structure diagnosis and CRC quantification (Son and Sivapalan, 2007; Birkel
63 et al., 2011), and are increasingly adopted in cold catchments (e.g., Ala-aho et al., 2017; He et
64 al., 2019; Nan et al., 2021a). Recent ~~researches~~ [studies](#) indicated that estimates of precipitation
65 $\delta^{18}\text{O}$ from outputs of isotopic general circulation models (iGCMs) perform well on forcing
66 tracer-aided models in large basins with a [high](#) ~~low~~ cost of water sampling (Delavau et al., 2017;
67 Nan et al. 2021b). Similarly to the tracer-based end-member mixing methods that utilize the
68 different tracer signatures of water sources to separate the hydrograph and quantify CRCs
69 (Klaus and McDonnell, 2013; He et al., 2020), the tracer-aided hydrological models used the
70 differed isotopic compositions of runoff components to ~~regulate~~ [constrain](#) the water
71 apportionments in runoff generation. The isotopic compositions of runoff components strongly
72 differ in high-mountain basins resulting from the following two reasons: One is the significantly
73 more depleted $\delta^{18}\text{O}$ of meltwater compared to that of rain, due to the altitude and temperature
74 effects, and the fractionation effect during melting processes (Xi, 2014; Boral and Sen, 2020).
75 Another is the damping and lagging isotopic variability of subsurface runoff pathway, compared
76 to that of surface runoff, as a result of the catchment hydrological functions of storing, mixing
77 and transporting water (Bowen et al., 2019; Birkel and Soulsby, 2015; McGuire and McDonnell,
78 2006). Consequently, water isotope signatures ~~bear good~~ [show](#) potentials to improve the
79 representations of internal hydrological processes in hydrological models, if observations of
80 water isotopes were involved in the model calibration and evaluation procedures (McGuire et

81 al., 2007; He et al., 2019).

82 Although a plenty of isotope-based works have been conducted in mountainous
83 catchments on the TP to improve understandings of local hydrological processes (e.g., Li et al.,
84 2020; Kong et al., 2019; Tan et al., 2021), ~~bare few~~ of them provided guidance on data collection
85 of water isotope for hydrological applications in large mountainous areas. Some water sampling
86 works in large mountainous catchments were conducted in a single field campaign (e.g., Xia et
87 al., 2019; Dong et al., 2018), which is, although helpful to understand the generations of short-
88 term runoff events, not suitable for the calibration of tracer-aided models in a multi-year
89 simulation period (Knapp et al., 2019; Zhang et al., 2019). An exception is Stevenson et al.
90 (2021) who utilized a 7-year dataset of stream water $\delta^{18}\text{O}$ in a 3.2 km² catchment to analyze the
91 effects of stream water sampling strategies on the calibration of a tracer-aided hydrological
92 model. Challenges arise when transferring their findings to the application of tracer-aided
93 hydrological models in large high-mountain basins: First, it is questionable that whether
94 sampling stream water at one site can adequately represent the isotope signature of stream water
95 over the whole large basin, considering the strong spatial variability of hydrological processes
96 caused by the heterogeneity in meteorological factors and land surface conditions in mountains
97 (Wang et al., 2021; Li et al., 2020). Second, the influences of data collection of precipitation
98 isotope on the performance of tracer-aided hydrological models remain unclear. Results of He
99 et al. (2019) indicated that monthly sampling of precipitation at two sites seems to be able to
100 capture the isotope variations in a 233 km² catchment. However, the requirement of isotope
101 data quantity to adequately capture the spatial pattern of precipitation isotope signature for
102 forcing tracer-aided models in large basins ($\sim 10^5$ km²) is poorly explored (Nan et al., 2021b).
103 Third, in glacierized mountainous catchments where streamflow was fed by additional water
104 source of glacier melt, the requirement of glacier meltwater samples for the forcing and
105 evaluation of tracer-aided hydrological models is also unclear. Consequently, better
106 understandings of how water sampling strategies influence the value of water isotope data for
107 aiding hydrological modeling, is highly helpful for guiding the establishment of monitoring
108 systems of water isotope in large mountainous regions. Considering the high costs of human
109 and financial resources of collecting water samples in TP area, it is important to take efficient
110 strategies for water sampling that balance the trade-off between field work burden and data
111 adequacy well (Sprenger et al., 2019).

112 Motivated by the mentioned backgrounds, we conducted detailed analysis on the tracer-
113 aided model performance in a large mountainous basin on the TP under different assumed
114 situations with respect to the collection strategy of site water isotope data, based on a numerical
115 experiment method. We adopted the tracer-aided hydrological model THREW-T developed by
116 Nan et al. (2021a), which was forced by the global gridded isotope outputs of iGCM being
117 ~~corrected by~~merged with measurements of precipitation $\delta^{18}\text{O}$, to achieve the research aim.

118 Three specific questions were addressed: (1) how does the estimated isotopic composition of
119 glacier meltwater influence the performance of tracer-aided hydrological modeling when no
120 glacier meltwater samples were available, (2) how does the collection strategy of site
121 precipitation samples ~~for the correction of iGCM~~ for precipitation isotope data merging
122 influence the model performance, and (3) how does the sampling strategy of stream water
123 influence the model calibration and evaluation?

124 **2. Materials and methodology**

125 **2.1 Study area**

126 The Yarlung Tsangpo River (YTR) basin, located in the southern TP (Fig. 1), extends in
127 the ranges of 27°N -32°N and 82°E -97°E, with an elevation extent of 2900-6900 m above sea
128 level (a.s.l.), which is one of the largest basins on the TP. The mean annual precipitation in the
129 YTR basin is around 470mm featured by a distinct wet season from June to September, due to
130 the dominance of the South Asian monsoon. Drainage area above the Nuxia hydrological station
131 at the basin outlet is approximately 2×10^5 km², ~~and~~ around 2% of which is covered by glacier.

132 The Karuxung River (KR) catchment is located in the upper regions of the YTR basin, and
133 was chosen as a supplementary experiment catchment, because of the long term field work of
134 water sampling in this catchment. The KR originates from the Lejin Jangsan peak of the Karola
135 mountain (7206m a.s.l.), and flows into the Yamdrok Lake (4550m a.s.l.), draining an area of
136 around 286 km². Streamflow in the KR catchment is strongly influenced by glaciers which
137 cover an area of 58 km².

138 **[Figure 1]**

139 **2.2 Hydro-meteorological and water isotope data**

140 Elevation of the YTR basin was derived from a digital elevation model (DEM) with a
141 spatial resolution of 30m from the Geospatial Data Cloud (<https://www.gscloud.cn>). Daily
142 meteorological inputs including precipitation, temperature and potential evapotranspiration
143 were collected from the 0.1°×0.1° China Meteorological Forcing Dataset (CMFD, Yang and
144 He, 2019). The second glacier inventory data set of China (Liu, 2012) was used to denote the
145 glacier coverage and was assumed to be constant during the study period. The seasonal snow
146 coverage was extracted from the Tibetan Plateau Snow Cover Extent product (TPSCE, Chen et
147 al., 2018), and was regarded as observation data for model calibration. ~~and the Tibetan Plateau~~
148 ~~Snow Cover Extent product (TPSCE, Chen et al., 2018) were used to denote the glacier and~~
149 ~~snow coverages.~~ Vegetation coverages were extracted from the MODIS satellite products of
150 eight-day leaf area index (LAI) dataset MOD15A2H (Myneni et al., 2015) and monthly
151 normalized difference vegetation index (NDVI) dataset MOD13A3 (Didan et al., 2015). Soil

152 types and properties in the tested basins were collected from the Harmonized World Soil
153 Database (HWSD, He, 2019). Observations of daily streamflow during 2000-2015 at the Nuxia,
154 and that during 2000-2010 at Yangcun and Nugesha stations were used for hydrological model
155 evaluation.

156 In the KR catchment, daily temperature and precipitation during 2006-2012 were collected
157 at the Langkazi meteorological station. Altitudinal distributions of temperature and
158 precipitation across the KR catchment were estimated based on the lapse rates reported in
159 Zhang et al. (2015). Daily streamflow during 2006-2012 was measured at the Wengguo
160 hydrological station.

161 Outputs of the scripps global spectral model with water isotopes incorporated (isoGSM,
162 Yoshimura et al., 2008) with the spatial and temporal resolutions of $1.875^\circ \times 1.875^\circ$ and 6h were
163 extracted to represent the spatio-temporal pattern of the precipitation isotope in the YTR basin.
164 According to ~~our a~~ previous evaluation of the isoGSM product (Nan et al., 2021b), it can well
165 capture the seasonal fluctuation of precipitation $\delta^{18}\text{O}$, but had two aspects of shortcomings:
166 overestimating precipitation $\delta^{18}\text{O}$ in the YTR basin, and performing poorly on capturing the
167 isotope signature of individual precipitation events and specific period. The bias of isoGSM
168 product tended to be larger in higher elevation regions.~~it overestimated precipitation $\delta^{18}\text{O}$ in the~~
169 ~~YTR basin (Nan et al., 2021b).~~ To ~~correct bias in the isoGSM products~~ obtain measurement
170 precipitation $\delta^{18}\text{O}$ data, grab samples of precipitation were collected in the wet season of 2005
171 at four stations along the main channel of YTR, i.e., Nuxia (3691 m a.s.l.), Yangcun (4541m
172 a.s.l.), Nugesha (4715m a.s.l.) and Lazi (4889m a.s.l.). The precipitation water samples were
173 collected as soon as possible after the precipitation event in order to avoid the effect of
174 evaporation. Stream water samples were collected weekly during the same period from river at
175 the four stations.

176 The isoGSM isotope products were merged with measurement precipitation isotope data
177 according to ~~corrected by~~ Eqs. 1-3 to provide input data for model: First, the bias of isoGSM
178 product was assumed to be linearly related to altitude. Relation between the mean bias of
179 isoGSM products and altitude was estimated by a least square method using $\delta^{18}\text{O}$ measurements
180 of precipitation samples and gridded isoGSM estimates at the four sampling sites (Eqs. 1-2);
181 Second, ~~on each grid of the isoGSM product~~ in each REW, precipitation $\delta^{18}\text{O}$ was determined
182 by Eq. 3, based on the average altitude and isoGSM estimate was corrected by a bias estimated
183 by the grid altitude in Eq. 3 based on the availability of $\delta^{18}\text{O}$ measurements from precipitation
184 site samples on the date.

$$185 \quad B_i = \overline{\delta^{18}\text{O}_{i,M}} - \overline{\delta^{18}\text{O}_{i,G}} \quad (1)$$

$$186 \quad B = a \cdot H + b \quad (2)$$

$$\delta^{18}O_{k,j,\text{MergedCorr}} = \begin{cases} \delta^{18}O_{k,j,G} + B_k, & \text{for date } j \text{ with no data} \\ \frac{\sum_{i=1}^4 \delta^{18}O_{i,j,M}}{4} - \frac{\sum_{i=1}^4 \overline{\delta^{18}O_{i,M}}}{4} + \overline{\delta^{18}O_{k,G}} + B_k, & \text{for date } j \text{ with data, but unit } k \text{ containing no sampling site} \\ \delta^{18}O_{k,j,M}, & \text{for date } j \text{ with data, and unit } k \text{ containing sampling site} \end{cases} \quad (3)$$

where, B_i is the bias of isoGSM at sites i . $\overline{\delta^{18}O_{i,M}}$ and $\overline{\delta^{18}O_{i,G}}$ are the weighted average of the site measurement and isoGSM estimate over the sampling period at sites i , respectively. H is the altitude of the sampling site. Parameters a and b are the linear regression coefficients, which were estimated as -0.0046 and 14.96 by the least square method in this study. $\delta^{18}O_{k,j,\text{MergedCorr}}$ is the ~~corrected isoGSM~~ precipitation isotope obtained by merging isoGSM and measurement data, and $\delta^{18}O_{k,j,G}$ refers to the original isoGSM isotope estimate at the hydrological model unit k on the date j .

Glacier meltwater $\delta^{18}O$ was assumed to be constantly lower than the weighted average of precipitation $\delta^{18}O$ by an offset parameter ($\Delta\delta$) during the study period (Eq. 4) because of the unavailability of glacier meltwater samples, which is generally within the range of 2-9‰ in the worldwide mountain regions (Rai et al., 2019; Wang et al., 2016; He et al., 2019; Ohlanders et al., 2013; Jeelani et al., 2017) and is adopted as 5‰ from Boral and Sen (2020) in the YTR basin.

$$\delta^{18}O_{k,GM} = \overline{\delta^{18}O_{k,Corr}} - \Delta\delta \quad (4)$$

In the KR catchment, grab samples of precipitation and stream water were collected at the Wengguo station in 2006-2007 and 2010-2012 for isotope analysis. The spatial distribution of precipitation $\delta^{18}O$ was estimated based on an altitudinal lapse of -0.34‰/100 as reported in Liu et al. (2007). Glacier meltwater $\delta^{18}O$ was assumed to be constantly as -18.9‰ during the study period (~~similarly to as reported by~~ Gao et al. 2009). Details of precipitation and stream water samples in the YTR and KR catchments were summarized in Table 1.

[Table 1]

2.3 Tracer-aided hydrological model

A distributed tracer-aided hydrological model, THREW-T (Tsinghua Representative Elementary Watershed - Tracer-aided version) model developed by Tian et al. (2006) and Nan et al. (2021a) was adopted for streamflow and isotope simulations. This model uses the representative elementary watershed (REW) method for spatial discretization of catchments (Reggiani et al., 1999). The study catchment is first divided into REWs based on DEM, and each REW is further divided into two vertical layers (surface and subsurface layers), including eight hydrological subzones based on the land cover and soil properties. In total, 63 and 41 REWs were extracted for the YTR basin and KR catchment, respectively (Tian et al., 2020;

220 Nan et al., 2021a, 2021b). Areal averages of the gridded estimates of meteorological variables,
221 vegetation cover and soil property were calculated in each REW to drive the model. A module
222 representing glacier melting and snowpack evolution was incorporated into the model for
223 application in cold regions (He et al., 2015; Xu et al., 2019; Tian et al., 2020; [Nan 2021a](#)).
224 [Accumulation and melting processes of snowpack were simulated according to temperature and](#)
225 [precipitation, to update snow water equivalent \(SWE\) of each REW. The snow cover area \(SCA\)](#)
226 [was then determined according to the snow cover depletion curve \(Fassnacht et al., 2016\) and](#)
227 [SWE threshold value \(Parajka and Blöschl, 2008\) for YTR basin and KR catchment,](#)
228 [respectively, due to the different catchment scales. The evolution of glacier was not simulated](#)
229 [in the model for simplification. The glacier melting amount was determined by the temperature-](#)
230 [index method and was assumed to contribute to streamflow through surface runoff pathway](#)
231 [directly.](#)

232 The tracer-aided module was developed by Nan et al. (2021a). [The isotope was assumed](#)
233 [to mix completely in each hydrological simulation unit within a simulation step. The Rayleigh](#)
234 [fractionation method was adopted to simulate the isotope fractionation during water](#)
235 [evaporation \(similarly to He et al. 2019, Hindshaw et al. 2011, Wolfe et al. 2007\). The isotope](#)
236 [concentration was updated according to the water content of each unit and fluxes among them,](#)
237 [which have been calculated by the hydrological model, thus no parameters associated to isotope](#)
238 [mixing was introduced.](#), ~~which simulated the isotope mixing and fractionation processes based~~
239 ~~on complete mixing assumption and Rayleigh fractionation method (similarly to He et al. 2019;~~
240 ~~Hindshaw et al., 2011; Wolfe et al., 2007).~~ Forced by the inputs of precipitation and glacier
241 meltwater isotopic compositions, the model simulates the isotope evolution in all the water
242 ~~sources storages~~ in the watershed, including stream water, soil water and snowpack. [The glacier](#)
243 [evolution processes were not simulated in the hydrological model, thus its isotope composition](#)
244 [cannot be updated by the model, and an assumed constant \$\delta^{18}\text{O}\$ of glacier melt was adopted to](#)
245 [calculate the isotope mass from glacier meltwater.](#) The iGCM isotope products properly
246 corrected by $\delta^{18}\text{O}$ measurements of precipitation samples have proved feasible to force the
247 THREW-T model in large catchments like YTR on the TP (Nan et al., 2021b). [More details of](#)
248 [hydrological model together with the snowpack evolution and tracer-aided module are given in](#)
249 [Tian et al. \(2006\) and Nan et al. \(2021a\)](#)

250 The THREW-T model quantified the contributions of runoff components (CRC) to
251 streamflow based on two definitions of runoff components as reviewed in He et al. (2021). The
252 first definition is based on the individual water sources in the total water input triggering runoff
253 processes, including rainfall, snowmelt and glacier melt. The second definition is based on
254 pathways of runoff-generation processes, resulting in surface and subsurface runoff (baseflow).
255 ~~More details of the model description and setup are given in Tian et al. (2006) and Nan et al.~~
256 ~~(2021a).~~

257 Physical basis and value ranges of the calibrated parameters in the THREW-T model were
 258 described in Table 2. The value of parameter was assumed to be universal for all the REWs.
 259 Two kinds of calibration approaches were conducted: (1) a bi-objective calibration using
 260 discharge and SCA, and (2) a tri-objective calibration using discharge, SCA and stream water
 261 $\delta^{18}\text{O}$. Metrics used to evaluate the model performance are listed in Eqs. 5-8. The Nash-Sutcliffe
 262 efficiency coefficient (NSE) was used to optimize the simulation of discharge and isotope,
 263 whereas the root-mean-square error (RMSE) was used for the evaluation of SCA simulation.
 264 The Logarithmic Nash-Sutcliffe efficiency coefficient (lnNSE) was used additionally for
 265 discharge calibration to assess the simulation of baseflow. The model parameters were
 266 calibrated by streamflow and SCA observations during 2001-2010 (at Nuxia station) and 2006-
 267 2012 in the YTR and KR basins, respectively. The model performance in YTR basin was
 268 evaluated-validated by the Nuxia streamflow and SCA observations during 2011-2015, and the
 269 streamflow observations at Yangcun and Nugesha stations during 2001-2010.

$$270 \quad \text{NSE}_{\text{dis}} = 1 - \frac{\sum_{i=1}^n (Q_{o,i} - Q_{s,i})^2}{\sum_{i=1}^n (Q_{o,i} - \bar{Q}_o)^2} \quad (5)$$

$$271 \quad \text{NSE}_{\text{Indis}} = 1 - \frac{\sum_{i=1}^n (\ln Q_{o,i} - \ln Q_{s,i})^2}{\sum_{i=1}^n (\ln Q_{o,i} - \ln \bar{Q}_o)^2} \quad (6)$$

$$272 \quad \text{RMSE}_{\text{SCA}} = \sqrt{\frac{\sum_{i=1}^n (\text{SCA}_{o,i} - \text{SCA}_{s,i})^2}{n}} \quad (7)$$

$$273 \quad \text{NSE}_{\text{iso}} = 1 - \frac{\sum_{i=1}^n (\delta^{18}\text{O}_{o,i} - \delta^{18}\text{O}_{s,i})^2}{\sum_{i=1}^n (\delta^{18}\text{O}_{o,i} - \bar{\delta}^{18}\text{O}_o)^2} \quad (8)$$

274 where, n is the total number of observations. Subscripts of “o” and “s” refer to observed and
 275 simulated variables, respectively.

276 An automatic algorithm Python Surrogate Optimization Toolbox (pySOT) developed by
 277 Eriksson et al. (2017) was adopted for the multiple-objective optimization. The pySOT
 278 algorithm used a surrogate model to guide the search for improved solutions, with the advantage
 279 of needing few function evaluations to find a good solution. In each pySOT running, the
 280 optimization procedure was stopped if a maximum number of allowed function evaluations was
 281 reached, which was set as 3000 in this study. For the bi- and tri-objective calibrations,
 282 $0.5 \cdot (\text{NSE}_{\text{dis}} + \text{NSE}_{\text{Indis}}) - \text{RMSE}_{\text{SCA}}$ and $0.5 \cdot (\text{NSE}_{\text{dis}} + \text{NSE}_{\text{Indis}}) - \text{RMSE}_{\text{SCA}} + \text{NSE}_{\text{iso}}$ were chosen as
 283 the combined optimization objectives. For each scenario, the pySOT algorithm was repeated
 284 100 times, and behavioral parameter sets were selected among the 100 final results according
 285 to the performance metric thresholds, i.e., only the parameter sets producing metrics better than
 286 certain threshold values were regarded as behavioral parameter sets. The model uncertainty was
 287 evaluated based on the model performance driven by the behavioral parameter sets. The
 288 threshold values of evaluation metrics were setused as $0.5 \cdot (\text{NSE}_{\text{dis}} + \text{NSE}_{\text{Indis}}) > 0.8$,
 289 $\text{RMSE}_{\text{SCA}} < 0.08$ in the YTR basin; and $\text{NSE}_{\text{dis}} > 0.7$, $\text{RMSE}_{\text{SCA}} < 0.15$ in the KR catchment.
 290 Different values were adopted for the NSE_{iso} threshold among different scenarios, which would

291 be introduced accordingly in the Result section.

292 [Table 2]

293 2.4 Numerical experiments

294 The influences of isotope data condition on model performance were evaluate in three
295 aspects as listed in Table 3: the assumed glacier meltwater isotope, the site measurement of
296 precipitation isotope for data merging, and the stream water sampling strategy for model
297 calibration.

298 [Table 3]

299 *Experiment 1: influence of assumed glacier meltwater isotope*

300 The first experiment was designed to test the reliance of model performance on the
301 assumed glacier meltwater isotope, as glacier melt water samples are typically not available for
302 isotope analysis in high mountain basins on the TP. In this experiment, variable glacier melt
303 isotope signatures were adopted to calculate the isotopic contribution from glacier meltwater to
304 streamflow used to force the model, assuming the glacier meltwater $\delta^{18}\text{O}$ is 1‰, 3‰, 7‰ and
305 9‰ (i.e., $\Delta\delta$ values in Table 3) lower than the long-term average $\delta^{18}\text{O}$ of precipitation. A
306 benchmark model running by the literature based $\Delta\delta$ value of 5‰ was used as a baseline
307 reference to assess the influence of the assumed glacier meltwater isotope on the model
308 performance.

309 *Experiment 2: influence of site measurement of precipitation isotope*

310 The second experiment was designed to test the reliance of the model performance on the
311 availability of measured site precipitation isotope that was merged with used to correct the
312 isoGSM product. The benchmark model running was forced by the corrected isoGSM merging
313 precipitation isotope data based on measurements of precipitation isotope from all the four
314 sampling sites (Figure 1). Three scenarios regarding the availability of measured precipitation
315 isotope were designed as shown in Table 3. First, we assumed that only precipitation isotope
316 measured at the two downstream sites of Nuxia and Yangcun are available for data merging the
317 correction of isoGSM (i.e., scenario P_2stationNY in Table 3). Second, we assumed that
318 precipitation isotope measurement at the most upstream site Lazi is available in addition to the
319 measurement at the downstream site Nuxia (i.e., scenario P_2stationNL in Table 3). Third, we
320 assumed that only precipitation isotope measurement at the most downstream site Nuxia is
321 available for the correction of isoGSM data merging (i.e., scenario P_1station in Table 3).

322 *Experiment 3: influence of stream water sampling strategy*

323 The third experiment was conducted to analyze the influence of stream water sampling
324 strategy on the model performance. Two types of stream water sampling strategies were

325 considered, i.e., a time series sampling strategy based on regular and continuous sampling work
 326 at a certain point, and a spatially distributed sampling strategy based on one-time field
 327 campaigns of sampling work. For the time series sampling strategy, 7 scenarios (scenarios begin
 328 with “RT_YTR_” in Table 3) were designed to analyze the influences of the sampling frequency,
 329 the duration of the sampling period, and the number of sampling sites. For the spatially
 330 distributed sampling strategy, two scenarios (Figure 1b) were designed to represent typical field
 331 campaign activities: collecting samples along the mainstream of the basin (RS_YTR_Main,
 332 Table 3), and collecting water samples additionally from major tributaries (RS_YTR_Tributary,
 333 Table 3). Considering the limited availability of stream water $\delta^{18}\text{O}$ measurement in the YTR
 334 basin (only wet season in one year, Table 1), a supplementary experiment was designed to test
 335 the influence of sampling period duration on the model performance using the relatively long
 336 time-series isotope dataset in the small catchment KR (scenarios begin with “RT_KR_” in Table
 337 3).

338 To evaluate the influence of isotope data availability on the model performance, we carried
 339 out benchmark model simulations forced by full datasets of input isotope and stream water
 340 isotope data in the YTR and KR catchments (Table 3). The benchmark model runs were
 341 calibrated by a bi-objective calibration using SCA and streamflow observations, and a tri-
 342 objective calibration using additional stream water isotope, respectively. It is noted that, in the
 343 scenarios of experiment 3 that were carried out in the YTR basin (i.e., scenarios starting with
 344 “RT_YTR” and “RS_YTR_” in Table 3), the assumed data availability was beyond the actual
 345 measurement dataset. Consequently, the assumed stream water $\delta^{18}\text{O}$ measurements were
 346 adopted from a model simulation driven by a benchmark parameter set (rather than a subset of
 347 actual measurement stream water $\delta^{18}\text{O}$), which was selected from the behavioral parameters of
 348 the BM_YTR scenario calibrated by tri-objective approach. It is noted that, in experiments that
 349 were carried out in the YTR basin (i. e., scenarios start with “RT_YTR_” and “RS_YTR_” in
 350 Table 3), assumed stream water $\delta^{18}\text{O}$ measurements were adopted from model simulations
 351 driven by a benchmark parameter set, which was selected from the behavioral parameters of
 352 the BM_YTR calibrated by tri-objective approach, because the assumed data availability was
 353 beyond the actual measurement dataset. The assumed stream water $\delta^{18}\text{O}$ measurements thus
 354 were not used to evaluate the model performance in simulating stream water isotope. Instead,
 355 the influence of the availability of stream water $\delta^{18}\text{O}$ measurement on the tracer-aided model
 356 were evaluated by comparing the estimated CRCs and corresponding uncertainties with the
 357 assumed true values that were derived from the tri-objective calibrated benchmark running.
 358 Mean absolute error (MAE) and standard deviation (STD) were used to quantify the accuracy
 359 and uncertainty of CRC, which were calculated in Eqs. 9 and 10.

$$360 \quad \text{MAE}^k = \frac{\sum_{i=1}^n |\text{CRC}_{s,i}^k - \text{CRC}_0^k|}{n} \quad (9)$$

361
$$\text{STD}^k = \sqrt{\frac{\sum_{i=1}^n (\text{CRC}_{s,i}^k - \overline{\text{CRC}_s^k})^2}{n}} \quad (10)$$

362 where, n is the number of behavioral parameter sets, and superscript k indicates the runoff
 363 component (one of rainfall, snowmelt, glacier melt and baseflow). Subscript s and o indicate
 364 the simulated and observed value (observed value is the CRC produced by the tri-objective
 365 calibrated benchmark running). $\text{CRC}_{s,i}^k$ is the contribution of runoff component k simulated by
 366 the parameter set i . $\overline{\text{CRC}_s^k}$ is the average CRC simulated by all the behavioral parameter sets.

367 In the scenarios of experiments 1 and 2 remaining experiments in Table 3, the model was
 368 calibrated towards the complete stream water $\delta^{18}\text{O}$ measurement dataset (Table 1), and the
 369 influence of isotope data availability on model performance were quantified by changes in
 370 model performance in the validation period and internal validate hydrological stations, as well
 371 as the uncertainty of CRC estimated by Eq. 10. In the scenarios of experiment 3 that were
 372 carried out in the YTR catchment (i.e., scenarios starting with “RT_YTR ” and “RS_YTR ”),
 373 a subset of simulated stream water $\delta^{18}\text{O}$ produced by the benchmark parameter set was picked
 374 out for model calibration. In the scenarios of experiment 3 that were carried out in the KR
 375 catchment (i.e., scenarios starting with “RT_KR ” in Table 3), a subset of stream water $\delta^{18}\text{O}$
 376 measurement dataset (Table 1) was picked out for model calibration.

377

378 3. Results

379 3.1 Performance of the tracer-aided hydrological model

380 Figure 2 shows performance of the benchmark model running (i.e., BM_YTR scenario in
 381 Table 3) forced and calibrated by the full available isotope dataset. The NSE_{iso} threshold by
 382 which behavioral parameter sets were selected in tri-objective calibration was set as 0.5.
 383 Seasonal variations in discharge and SCA were reproduced well by the bi-objective calibration
 384 (Figure 2a and 2b), indicated by the high values of NSE_{dis} (>0.8) and $\ln\text{NSE}_{\text{dis}}$ (>0.8), and a
 385 low RMSE_{SCA} (<0.08). The peak flows were less well reproduced by the model in comparison
 386 to the simulation of baseflow processes, partly due to the inaccurate precipitation input data at
 387 the high altitudes. The model showed extremely poor performance for the simulation of stream
 388 water isotope when looking at the large uncertainty range (Figure 2c) and low NSE_{iso} (-0.72).
 389 The tri-objective calibration significantly improved the isotope simulation (Figure 2f), without
 390 bringing much sacrifice to the performance in simulating discharge and SCA (considering the
 391 minimum values of NSE_{dis} and $\ln\text{NSE}_{\text{dis}}$ are around 0.7 in Figure 2d and 2e). Moreover, the tri-
 392 objective calibration slightly reduced uncertainty for simulation of the rising hydrograph in the
 393 2009 spring (Figure 2d). The seasonal variations in stream water $\delta^{18}\text{O}$ were captured well at all
 394 the four stations by simulations from the tri-objective calibration. The mean contributions of
 395 rainfall and snowmelt to annual streamflow estimated by the bi-objective calibration were 62.8%

396 and 10.8%, which were around 1%-7% smaller than those estimated by the tri-objective
397 calibration (Table 4). In contrast, the contribution of glacier melt estimated by the tri-objective
398 calibration (17.1%) was lower than that estimated by the bi-objective calibration (26.4%).
399 Surface runoff which was mainly fed by glacier melt in the YTR showed a larger proportion in
400 the total streamflow simulated by a bi-objective calibration (52.1%) than that in the simulation
401 of a tri-objective calibration (44.7%), while baseflow contribution quantified by the bi-
402 objective calibration is smaller. Standard deviation values of the quantified CRCs indicated that
403 the tri-objective calibration estimated smaller uncertainties for the quantifications of runoff
404 components.

405 **[Figure 2]**

406 **[Table 4]**

407 The uncertainty of behavioral parameter set obtained by bi- and tri-objective calibration is
408 shown in Figure 3. Apart from the hillslope roughness coefficient (m), the uncertainties of all
409 the parameters were reduced by tri-objective calibration to varying degrees, especially for the
410 parameters related to melting (DDF_N and T_0) and flow concentration processes ($C1$ and $C2$).
411 The higher melting temperature threshold (T_0) obtained by tri-objective calibration was
412 consistent with the lower contribution of melt water. The lower water storage capacity (WM)
413 and higher shape coefficient (B) of tri-objective calibration should resulted in higher saturation
414 area and consequently higher contribution of surface runoff, which was however not in
415 agreement with the estimated CRC, indicating the important contribution of glacier melt in
416 surface runoff. A benchmark parameter set that performed well on multiple objectives was
417 selected among the behavioral parameters of BM_YTR calibrated by tri-objective method (as
418 shown in Table 5), to produce stream water $\delta^{18}O$ for model calibration in experiment 3 in YTR
419 basin. It is noted that this benchmark parameter set was only used to produce stream water $\delta^{18}O$
420 data for model calibration in experiment 3 in YTR basin, not necessarily an optimal parameter
421 set representing the true hydrological processes.

422 **[Figure 2][Figure 3]**

423 **[Table 5]**

424 **[Table 4]**

425 **[Table 5]**

426 Figure 43 shows model performances in the KR catchment. The parameter sets producing
427 positive NSE_{iso} were selected as behavioral for tri-objective calibration. Variations of discharge
428 and SCA were reproduced comparably well by the bi- and tri-objective calibrations indicated
429 by the similar metric values. However, the bi-objective calibration produced extremely poor
430 performance for the isotope simulation with low NSE_{iso} and a large simulation error of $\sim 5\%$
431 (Figure 43c). The tri-objective calibration captured the seasonal variations in stream water $\delta^{18}O$
432 during the study period well. Similarly to YTR, the tri-objective calibration resulted in lower

433 uncertainty in the simulated hydrograph (e.g., early 2010, 2006 and 2008), benefiting from
434 involving isotope for the model calibration to reject parameter sets that produced good
435 performance for discharge and SCA simulations but poor performance for isotope simulation.
436 Regarding the CRCs to total streamflow, the bi-objective and tri-objective calibrations
437 estimated similar results with differences up to 3%. The mean contributions of rainfall,
438 snowmelt and glacier melt to annual streamflow in the KR catchment were around 45%, 22%
439 and 33%, respectively. Contribution of surface runoff estimated by the bi-objective calibration,
440 however, was 13% lower than that estimated by the tri-objective calibration. In contrast,
441 baseflow is more important in the total streamflow simulated by the bi-objective calibration
442 (accounting for 38%) in comparison to the simulation of the tri-objective calibration
443 (accounting for 25%). Again in the KR catchment, uncertainties of CRCs quantified by the tri-
444 objective calibration are much smaller than those estimated by the bi-objective calibration
445 ([Table 4](#)[Figure 3](#)).

446 **[Figure 43]**

447 **3.2 Changes in model simulations forced by different assumed glacier meltwater isotopes**

448 Behavioral parameter sets of experiment 1 were selected based on the same NSE_{iso}
449 threshold (0.5) with the benchmark running. Model simulations forced by assumed glacier
450 meltwater $\delta^{18}O$ that are 5‰ (scenario BM_YTR, $\Delta\delta=5\text{‰}$) and 7‰ (scenario G_Δ7, $\Delta\delta=7\text{‰}$)
451 lower than the long-term average precipitation $\delta^{18}O$ showed the best discharge simulations in
452 the validation period (2011-2015) and stations (Yangcun and Nugesha), indicated by the high
453 average metric values (Figure 45). It is noted that simulations of all the glacier meltwater
454 isotope input scenarios in experiment 1 except G_Δ1 performed better than the bi-objective
455 calibration in which isotope data was not involved for parameter ~~identification~~optimization.
456 The model in the scenario G_Δ1 performed better on discharge simulation for validation period
457 (Figure 5a), but worse for internal stations (Figure 5b and 5c) than the result obtained by bi-
458 objective calibration.

459 ~~Discharge simulation in the scenario of G_Δ1 estimated higher performance in the~~
460 ~~validation period than the bi-objective calibration (Figure 4a), but lower performance at internal~~
461 ~~stations (Figure 4b and 4c).~~

462 **[Figure 45]**

463 Figure 5-6 shows the average CRCs and corresponding uncertainties estimated by the
464 different glacier melt isotope inputs. Scenarios with larger $\Delta\delta$ values (i.e., glacier meltwater
465 isotope is much lower than precipitation isotope) tended to result in higher contributions of
466 precipitation and lower contributions of glacier melt (Figure 56). This can be expected, as
467 stream water $\delta^{18}O$ is a mixture mainly from $\delta^{18}O$ of precipitation and glacier meltwater in YTR
468 basin and precipitation $\delta^{18}O$ is fixed in all the scenarios. Result of scenario G_Δ1, however,

469 estimated a smaller contribution of glacier melt than the scenario G_Δ3. This was likely due to
470 that the behavioral parameter sets were selected based on the performance of both discharge
471 and isotope simulations. Parameter sets that estimated higher glacier melt contribution with
472 good performance in isotope simulation but performed poorly on discharge simulation were
473 excluded from the behavioral set in the G_Δ1 scenario.

474 **[Figure 56]**

475 **3.3 Changes in model performance forced by ~~corrected~~ isoGSM product merged** 476 **with using different site measurements of precipitation isotope**

477 Figure 7 shows the relationship between REW-scale weighted averages of precipitation
478 δ¹⁸O and the longitude/elevation of corresponding REW for the scenarios in experiment 2. The
479 precipitation δ¹⁸O showed similar spatial pattern in the scenarios merging isoGSM with
480 measurement data at more than one sites. In scenario P_1station that merged isoGSM with
481 measurement data only at the most downstream station Nuxia, however, spatial pattern was
482 different, showing as significantly higher precipitation δ¹⁸O than other scenarios. The different
483 precipitation δ¹⁸O pattern was mainly a result of different altitudinal lapse rates of the isoGSM
484 bias (i.e., parameter *a* in equation 2). Representing the bias characteristic in the whole basin
485 solely by the data measured at the most downstream station resulted in significantly
486 underestimated isoGSM bias, and consequently overestimated precipitation δ¹⁸O.

487 Different precipitation δ¹⁸O input data inevitably resulted in different simulations of stream
488 water δ¹⁸O as shown in Figure 8. The NSE_{iso} threshold was set as 0.5 except for scenario
489 P_1station, which produced extremely poor δ¹⁸O simulation due to the high bias in merged
490 precipitation δ¹⁸O input data (Figure 8d). The other three scenarios all perform well in stream
491 δ¹⁸O simulation (Figure 8a-c), among which scenario P_2stationNL produced highest behavior,
492 followed by P_4station and P_2stationNY.

493 **[Figure 7]**

494 **[Figure 8]**

495 Different precipitation isotope input data also led to different performance in hydrological
496 modeling (Figure 9). While different scenarios produced similar SCA simulations in the
497 validation period (Figure 96d), the performance of discharge simulation significantly differed
498 among the precipitation isotope input scenarios ~~in experiment 2~~. In scenarios BM_YTR and
499 P_2stationNL, the model performed better than the bi-objective calibration in the validation
500 period (Figure 96a) and stations (Figure 69b and 96c), showing higher average values and
501 smaller ranges of NSE_{dis}, which indicated that the model benefitted from involving isotope data
502 for calibration. The model performance forced by scenario P_2stationNY was close to that of
503 the bi-objective calibration, with poorer discharge simulation at internal stations (Figure 9b and
504 9c). Using precipitation isotope input from the scenario P_1station, however, the model

505 performance was significantly worse than that of the bi-objective calibration. Reasons for the
 506 variable model performance forced by the precipitation isotope input scenarios could be: Site
 507 measurements of precipitation isotope used in scenarios BM_YTR (using data at four sampling
 508 stations) and P_2stationNL (using data at the most downstream sampling station and the most
 509 upstream sampling station) tended to provide more informative spatial distribution of
 510 precipitation $\delta^{18}\text{O}$ in the basin and were the most valuable data for the ~~correction of isoGSM~~
 511 ~~estimate precipitation isotope data merging~~; in the scenario of P_1station, on the contrary, the
 512 ~~bias of isoGSM product was inadequately corrected by site precipitation isotope measured only~~
 513 ~~at the most downstream station Nuxia, resulting in much errors in the isoGSM product at high~~
 514 ~~altitudes. Although precipitation isotope input data did not influence simulation of hydrological~~
 515 ~~processes, the calibration process that attempted to match simulated stream $\delta^{18}\text{O}$ with~~
 516 ~~measurement influenced the parameter, and consequently affected the internal hydrological~~
 517 ~~processes.-~~

518 **[Figure 96]**

519 Figure 7-10 shows the average CRCs and corresponding uncertainties estimated by the
 520 different precipitation isotope input scenarios. All scenarios produced lower uncertainties than
 521 the bi-objective calibration, which can be expected as they were calibrated by a tri-objective
 522 approach. The variable precipitation input scenarios resulted in contribution differences of
 523 around 10% in runoff components of rainfall, glacier melt and baseflow. ~~The sort of estimated~~
 524 ~~contribution of rainfall ($P_{2stationNL} > BM_YTR > P_{2stationNY} > P_{1station}$) was opposite~~
 525 ~~to that of average precipitation $\delta^{18}\text{O}$ shown in Figure 7, which was as expected according to an~~
 526 ~~estimation based on the end-member mixing method.~~

527 ~~Different site measurements of precipitation isotope that were used for the correction of~~
 528 ~~isoGSM product resulted in different altitudinal lapse rates in the corrected isoGSM input (i.e.,~~
 529 ~~parameter a in equation 2); and scenario P_1station estimated the most overestimated average~~
 530 ~~precipitation $\delta^{18}\text{O}$ ($\overline{\delta^{18}\text{O}_{precipitation}}$), while scenario P_2stationNL estimated the lowest~~
 531 ~~$\overline{\delta^{18}\text{O}_{precipitation}}$, leading to varied precipitation contributions to streamflow.—~~

532 **[Figure 710]**

533 Among the evaluation metrics, discharge simulation at Nugesha station showed the largest
 534 sensitivity to precipitation isotope inputs. As shown in Figure 8-11, scenarios P_2stationNY and
 535 P_1station estimated higher contribution of meltwater, earlier discharge onset timing and higher
 536 peak flow. The discharge began to rise especially early (around February) in scenario P_1station,
 537 because of the low calibrated value for the melting temperature threshold T_0 (-4.5°C), resulted
 538 in extremely poor discharge simulation (average NSE is around 0, Figure 8-11d).

539 **[Figure 811]**

540 3.4 Model performance constrained by different stream water sampling strategies

541 Figure 129 shows the accuracy and uncertainty metrics of CRCs produced by experiment
542 3 in the YTR basin. The NSE_{iso} threshold was set as 0.8, because the stream isotope data for
543 model calibration was generated by a benchmark parameter set, towards which good simulation
544 was rather easy to produce. In comparison to the baseline scenario of RT_TYR_BM, collecting
545 stream isotope data in the dry season (i.e., from November to next February in scenario
546 RT_YTR_WholeYear) brought little benefits to the estimation of water sources proportions, but
547 significantly improved the quantifications of runoff generation pathways indicated by the lower
548 MAE and STD in Figure 9b. The stream water in dry season was fed mainly by groundwater.
549 Stream water isotope data collected in this period reflect the release of groundwater storage,
550 thus helping to constrain the partition between surface and subsurface runoff pathway. On the
551 other hand, reducing the frequency of stream isotope data from weekly to monthly (i.e., scenario
552 RT_YTR_Monthly) led to significantly higher MAE and STD for both the partitions of water
553 sources and runoff pathways, which indicated that stream water isotope data collected by a
554 monthly sampling strategy could provide less constrains to model calibration. Extending the
555 duration of stream isotope sampling period by one or two years (i.e., scenarios RT_YTR_2year
556 and RT_YTR_3year) did not bring much benefits to the quantifications of CRCs regarding the
557 similar metric values. Using stream water isotope data from a three years' sampling
558 (RT_YTR_3year) even led to higher MAE and STD than that using stream water isotope data
559 from a 2 years' sampling (RT_YTR_2year), which might be an occasional result obtained by
560 the random calibration procedure (100 pySOT runs). In comparison to simulations constrained
561 by stream water isotope data from multiple sampling years, results constrained by stream water
562 isotope data from multiple sampling sits (i.e., scenarios of RT_YTR_2station and
563 RT_YTR_4station) yielded lower MAE and STD for the quantified CRCs.

564 [Figure 912]

565 Model simulations calibrated by spatially distributed stream $\delta^{18}O$ data collected in a one-
566 time field campaign reduced the CRC uncertainty compared to the bi-objective calibration
567 (Figure 129). However, its MAE and STD for the quantifications of CRCs were higher than
568 that estimated by the model when calibrated by weekly sampled time series of stream $\delta^{18}O$.
569 Additionally using stream isotope data from four major tributaries (i.e., scenario
570 RS_YTR_Tributary) brought little benefits to the model performance than using isotope data
571 from the main stream solely (RS_YTR_Main), partly due to the signatures of stream water
572 isotope from tributaries were already reflected by water samples collected at confluences on
573 the main river channel.

574 In the KR catchment, stream isotope data was collected from five continues years,
575 providing better data basis for the evaluation of the influence of sampling period duration. The

576 NSE_{iso} threshold was set as 0, same with the benchmark scenario in KR catchment. Figure 130
577 and 141 compare the CRC estimations and their uncertainty metric STD of variable scenarios.
578 For the estimate of water sources, the model produced rather large uncertainty ranges of ~20%
579 and ~40% for the contributions of rainfall and glacier melt when calibrating the model using
580 discharge and SCA. Using one-year's stream water isotope data for model calibration, the
581 uncertainty ranges were reduced by rejecting some outliers as shown in Figure 10a-c, but the
582 STD was still large (Figure 131). The STD can be reduced by increasing the number of
583 calibration isotope data at a rate of ~1%/year. Using isotope data collected from five years,
584 however, didn't result in further decrease in the CRC uncertainties compared to the result
585 calibrated by isotope data collected in a four-year sampling period. The situation, however, was
586 quite different for the estimates of runoff pathways. The bi-objective calibration produced a
587 large uncertainty of ~40% and a STD of ~10% (Figure 130d) for the contribution of baseflow.
588 Using one-year's data for model calibration, the uncertainty range was significantly reduced by
589 about half of that modelled by the bi-objective calibration (from ~10% to ~5%). However,
590 further increase in the duration of sampling period did not bring much improvements on
591 constraining the uncertainties in quantifications of runoff pathways with STD fluctuating
592 around only 4%. It is indicated that model calibration upon more stream isotope data was useful
593 to better constrain the uncertainties of the model simulations and modeled CRCs, but benefit
594 would disappear after a certain duration of stream water sampling period has been reached.

595 [Figure 130]

596 [Figure 141]

597 4. Discussions

598 4.1 Implications for water sampling for isotope analysis in high mountains of TP

599 This study tested the reliance of the benefits of using tracer-aided hydrological model on
600 isotope data availability in two mountainous catchments YTR and KR on the TP. Our findings
601 consistently showed that the model robustness, with respect to performance in the validation
602 period and internal stations and the quantifications of CRCs, can be significantly improved by
603 involving isotope data for parameter calibration, similarly to previous tracer-aided modeling
604 studies (e.g., He et al., 2019; Ala-aho et al., 2017; Birkel et al., 2010). It can be expected that
605 more data help to provide more constrains on identification of model parameters. Nonetheless,
606 water sampling in high mountains on the TP is restricted by environment accessibility, financial
607 and human costs (Stevenson et al., 2021, Li et al., 2020). It is therefore highly needed to find
608 optimal strategies of collecting water samples that balance well between data adequacy for
609 model running and affordable sampling cost (Sprenger et al., 2019).

610 As an important water source in mountainous catchment on the TP, sampling of glacier

611 meltwater was expected to be favorable for the determination of glacier meltwater isotopic
612 composition and its contribution to total streamflow (He et al., 2019). Field campaign for
613 sampling of glacier melt water is strongly challenging in the YTR basin in this study, due to the
614 harsh accessibility of very high altitudes where glaciers lie. We thus assumed that glacier
615 meltwater $\delta^{18}\text{O}$ was lower than the average local precipitation $\delta^{18}\text{O}$ by an offset parameter ($\Delta\delta$).
616 This simple assumption turned to work well on driving the tracer-aided hydrological model and
617 produced better performance than the bi-objective calibration in both validation periods and
618 internal stations. Experiments by using different $\Delta\delta$ values indicated that the prior assumed
619 isotopic compositions of glacier melt have small influence on the estimated glacier meltwater
620 contribution in the YTR basin. It should be noted that this was different from the results of some
621 hydrograph separation works (e.g., Pu et al., 2020; Lone et al., 2021), which indicated that the
622 change of meltwater isotope composition would lead to significant difference in the
623 contribution of runoff component. Those works were based on the end-member mixing
624 approach, which was applied in a short time scale, and was more dependent on the isotope
625 composition of each runoff component. However, this work applied the tracer-aided
626 hydrological model in a longer time scale, where the temporal variability of isotope
627 composition played a more important role than its absolute value, on the parameter calibration.
628 Consequently, when the temporal variability of isotope composition of each water source was
629 reproduced properly, the glacier melt $\delta^{18}\text{O}$ value in a reasonable range would have little
630 influence on the model performance. The $\Delta\delta$ values ranging from 2‰-9‰ led to only ~5%
631 difference in the estimated contributions of glacier melt. Using a $\Delta\delta$ to estimate glacier
632 meltwater $\delta^{18}\text{O}$ could serve as an option to force the tracer-aided hydrological models in high-
633 mountain catchments where collecting glacier meltwater samples is highly challenging.

634 Results of experiment 2 indicated that the original isoGSM precipitation $\delta^{18}\text{O}$ data showed
635 large bias in the high mountain basins on TP, and must ~~undergo correction~~ be corrected by
636 measurement data before using to force the tracer-aided hydrological model. Our experiments
637 showed that measurement of precipitation isotope at only two sampling sites (scenario
638 P_2stationNL) in the large YTR basin of $2 \times 10^5 \text{ km}^2$ can be highly valuable for ~~the correction~~
639 ~~of isoGSM product~~ isotope data merging. Forced by isoGSM data that was ~~corrected by merged~~
640 with precipitation $\delta^{18}\text{O}$ measurements from two sampling sites, the model performed better than
641 the bi-objective calibration in simulating discharge in the validation period and internal stations,
642 and performed comparably to the simulations of a benchmark running which used precipitation
643 $\delta^{18}\text{O}$ measurements from four stations for the ~~isoGSM correction~~ data merging. This benefitted
644 from the large altitudinal range covered by the two sampling sites (a most downstream site
645 Nuxia and a most upstream site Lazi) to represent the spatial pattern of isoGSM bias. Likewise
646 using measurement data at two sites in the scenario P_2stationNY, model performance
647 deteriorated visibly, as the sampling sites (Nuxia and Yangchun) were both located in the

648 downstream regions, being worse at representing the spatial pattern of precipitation $\delta^{18}\text{O}$ over
649 the basin. Consequently, the strategy of collecting precipitation samples [for isotope data](#)
650 ~~merging to correct isoGSM~~ should be carefully designed; spending high cost on collecting
651 precipitation samples within a small region might be not worth at improving the performance
652 of the tracer-aided hydrological model.

653 Measurements of stream water $\delta^{18}\text{O}$ are essential for the calibration and evaluation of
654 tracer-aided hydrological models. Three kinds of sampling strategies in YTR basin were
655 evaluated in experiment 3: one-time campaign field sampling, continuous sampling at a fixed
656 location for a long period, and continuous sampling at multiple fixed locations during a short
657 period. It is indicated that continuously sampled stream water $\delta^{18}\text{O}$ at a fix location is more
658 valuable for aiding hydrological model than that collected by one-time field sampling
659 campaigns at distributed sites. Seasonality of stream water $\delta^{18}\text{O}$ referring to the processes of
660 water storage, mixture and transport in the basin can be better captured by continuous time
661 series measurements of $\delta^{18}\text{O}$ data (McGuire and McDonnell, 2006). Spatially sampled stream
662 water $\delta^{18}\text{O}$ data by one-time field sampling campaigns possibly miss seasonal $\delta^{18}\text{O}$ signatures
663 of stream water that were caused by seasonal runoff generation processes (Kendall and Coplen,
664 2001; Nan et al., 2019), and provide less constrains for the model calibration. Sampling of
665 stream water during dry season (scenario RT_YTR_WholeYear) brought little improvements
666 to the modeling of water source proportions, which is consistent with the findings in Stevenson
667 et al. (2021). High [frequent frequency](#) like weekly sampling of stream water in the dry season
668 makes small senses on improving the stream $\delta^{18}\text{O}$ data quality, as stream $\delta^{18}\text{O}$ in this season
669 has little variations due to small precipitation triggered runoff inputs. Monthly sampling of
670 stream water (RT_YTR_Monthly) turned to be insufficient to capture the strong hydrological
671 variations in the wet season (Birkel and Soulsby, 2015). For large basins like YTR, increasing
672 the number of sampling site for stream water $\delta^{18}\text{O}$ is more useful than extending the years of
673 sampling period at fixed sites, as seasonality of $\delta^{18}\text{O}$ signatures of water sources should be
674 similar among years in a short study period. Consequently, continuous sampling at multiple
675 locations in a short period like one or two years seems to be the optimal stream sampling
676 strategy for running tracer-aided hydrological model in mountainous basins like YTR on the
677 TP. The value of extending sampling period was more significant in a smaller catchment KR.
678 The uncertainty of CRC estimation kept decreasing until the data series length reached four
679 years and two years, for the aspects of water source and runoff pathway, respectively. This was
680 consistent with the finding by Stevenson et al. (2021) that the benefits from isotope plateaued
681 after a certain year number, which was five for that study.

682 4.2 Uncertainties and limitations

683 This study used simulated stream $\delta^{18}\text{O}$ [produced by](#) a benchmark [parameter set \(Table](#)

684 5)model running to represent the fully available dataset of stream $\delta^{18}\text{O}$ for water sampling in
685 the YTR basin, due to the limited stream water samples. This procedure likely caused the
686 inherent correlation of the stream $\delta^{18}\text{O}$ dataset, which made the model easily reproduce the
687 assumed measurements of stream $\delta^{18}\text{O}$ and may underestimate the value of stream $\delta^{18}\text{O}$ data
688 collected in extended sampling years and sampling sites. Results in this study serve to provide
689 preliminary understandings of the influences of stream water sampling strategy on the model
690 performance. More solid evaluations, however, can be further benefited from using more real
691 field measurements of stream $\delta^{18}\text{O}$ in the mountain basins.

692 Our study tried to look for optimal water sampling strategies to provide isotope input and
693 calibration data for the tracer-aided hydrological model in the YTR basin and KR catchment on
694 the TP. The transferability of our findings to other basins can be partly expected. For example,
695 we can expect that in catchments where precipitation $\delta^{18}\text{O}$ and runoff processes show small
696 spatial heterogeneity, collecting water samples at multiple stations would bring few additional
697 benefits for the modeling work than collecting water samples at a sole station. The influence of
698 assumed glacier meltwater would differ with the glacier covered area fraction in the basins.
699 However, situations in catchments with different geographical and climatic characteristics were
700 not evaluated in this study, which is restricted by the fact that high-quality water isotope data
701 in a set of mountain basins on the TP were hardly available currently (Birkel and Soulsby, 2015).
702 The authors suggest tracer-aided modeling researchers to publish their water isotope data to
703 improve the evaluation of the reliance of tracer-aided modeling performance on water sampling
704 strategy (similarly to He et al. 2021; Niinikoski et al., 2016; Yde et al., 2016).

705 The model performances were evaluated based on the behavioral parameter sets, which
706 were selected by the threshold values of evaluation metrics. The threshold values were
707 determined by looking at the graph comparing simulation and observation values, and
708 artificially judging whether good fitness has been achieved. This process was rather subjective,
709 and had inevitable influence on the evaluation result. However, this was widely used method
710 (e.g., Birkel et al., 2011; Delavau et al., 2017; He et al., 2019), and the threshold values were
711 set at levels achieved by the studies conducted in the same region (e.g., Zhang et al., 2015;
712 Chen et al., 2017), thus the model evaluation process has little influence on the key conclusions
713 of this study.

714 Another limitation of the model was the lack of isotope data for snow and glacier melt
715 water. Previous researches indicated that the spatio-temporal variability of melt water isotope
716 composition has important influence on the estimated contribution of runoff components (Pu et
717 al., 2020; Lone et al., 2021). Although the spatio-temporal variability of melt water isotope was
718 characterized in the model by simulating the isotope composition of snowpack storage, and
719 estimating the glacier melt isotope according to the average local isotope composition of
720 precipitation, it was difficult to valid whether they were characterized properly due to the data

721 limitation. We could only infer that the simulation of melt water isotope was acceptable, by the
722 fact that the model performs better on the simulation of discharge and stream isotope at both
723 outlet and internal stations, compared to the result obtained by bi-objective calibration without
724 calibrating isotope. More data of melt water isotope would be helpful to verify the isotope
725 simulation and estimation of CRC.

726 **5. Conclusion**

727 The value of water isotope data for aiding hydrological modeling in large mountainous
728 catchments was tested by a set of numerical experiments in the YTR basin. Reliance of the
729 tracer-aided model performance on the availability of input isotope data and evaluation stream
730 water isotope data was extensively investigated in the numerical experiments. Results could
731 provide important guidance for collecting water sampling and establishing tracer-aided
732 hydrological model in mountainous regions on the TP. Our main finds are as follows:

733 1. In high-mountain basins where glacier meltwater samples for isotope analysis are not
734 available, estimating isotopic composition of glacier meltwater by an offset parameter from
735 precipitation isotope is a feasible way to force the tracer-aided hydrological model. Our test
736 indicated that using a set of glacier meltwater $\delta^{18}\text{O}$ that are 2‰~9‰ lower than the mean
737 precipitation $\delta^{18}\text{O}$, resulted in small changes in the model performance and the quantifications
738 of CRCs (smaller than 5%) in the YTR basin. This influence, however, is expected to change
739 with the glacier area coverages in other mountain basins.

740 2. Strategy of field sampling for precipitation to collect measurement precipitation $\delta^{18}\text{O}$
741 merged with ~~correct~~ the isoGSM product should be carefully designed. Collecting precipitation
742 samples at sites from the same altitude tends to be worse at representing the spatial pattern of
743 precipitation $\delta^{18}\text{O}$ over the basin than collecting precipitation samples from sites covering a
744 range of altitudes. Measurements of precipitation isotope at only two sampling sites covering
745 an elevation range of 2900-6900m in the large YTR basin of $2 \times 10^5 \text{ km}^2$ can be highly valuable
746 for the correction of isoGSM product precipitation isotope data merging.

747 3. Collecting weekly stream water samples at multiple sites in the wet and warm seasons is
748 the optimal strategy to capture more hydrological process variability for calibrating and
749 evaluating a tracer-aided hydrological model in the YTR basin. It is highly recommended to
750 increase the number of stream water sampling sites in the high-mountain basins rather than
751 extending the duration of sampling period at a sole site. Benefits from extending the duration
752 of sampling period is more visible in a small catchment but smaller in large basins, and tend to
753 disappear when a certain duration of sampling period has been reached.

755 **Code and data availability**

756 Code and data availability. The isotope data and the code of THREW-T model used in this study

757 are available from the corresponding author (tianfq@tsinghua.edu.cn). Other data sets and the
758 calibration program pySOT are publicly available as follows: DEM
759 (<http://www.gscloud.cn/sources/details/310?pid=302>, last access: 1 January 2019, Geospatial
760 Data Cloud Site, 2019), CMFD (<https://doi.org/10.11888/AtmosphericPhysics.tpe.249369.file>,
761 Yang and He, 2019), glacier data (<https://doi.org/10.3972/glacier.001.2013.db>, Liu et al., 2012),
762 NDVI (<https://doi.org/10.5067/MODIS/MOD13A3.006>, Didan et al., 2015), LAI
763 (<https://doi.org/10.5067/MODIS/MOD15A2H.006>, Myneni et al., 2015), HWSD
764 (<https://data.tpdc.ac.cn/zh-hans/data/3519536a-d1e7-4ba1-8481-6a0b56637baf/?q=HWSD>,
765 last access: 1 January 2019, He, 2019) and the pySOT program
766 (<https://doi.org/10.5281/zenodo.569554>, Eriksson et al., 2017). These data sets and programs
767 are also referred to in the main text (Yang et al., 2010; Chen et al., 2018).

768 **Author contribution**

769 YN, ZH and FT conceived the idea; ZW provided the isoGSM data; LT provided the
770 measurement isotope data; YN, ZH and FT conducted analysis; ZW and LT provided comments
771 on the analysis; all the authors contributed to writing and revisions.

772 **Financial support**

773 This study has been supported by the National Natural Science Foundation of China (grant no.
774 92047301).

775 **Competing interests**

776 At least one of the (co-)authors is a member of the editorial board of Hydrology and Earth
777 System Sciences.

778

779 **References**

780 Ala-aho, P., Tetzlaff, D., McNamara, J. P., Laudon, H., and Soulsby, C.: Using isotopes to
781 constrain water flux and age estimates in snow-influenced catchments using the STARR
782 (Spatially distributed Tracer-Aided Rainfall–Runoff) model, *Hydrology and Earth System
783 Sciences*, 21, 5089–5110, 10.5194/hess-21-5089-2017, 2017.

784 Birkel, C., Dunn, S. M., Tetzlaff, D., and Soulsby, C.: Assessing the value of high-resolution
785 isotope tracer data in the stepwise development of a lumped conceptual rainfall-runoff
786 model, *Hydrological Processes*, 24, 2335–2348, 10.1002/hyp.7763, 2010.

787 Birkel, C., Tetzlaff, D., Dunn, S. M., and Soulsby, C.: Using time domain and geographic source
788 tracers to conceptualize streamflow generation processes in lumped rainfall-runoff models,
789 *Water Resources Research*, 47, 10.1029/2010wr009547, 2011.

790 Birkel, C., and Soulsby, C.: Advancing tracer-aided rainfall-runoff modelling: a review of

791 progress, problems and ~~unrealise~~ unrealized potential, *Hydrological Processes*, 29, 5227-
792 5240, 10.1002/hyp.10594, 2015.

793 Bloeschl, G., and Montanari, A.: Climate change impact: throwing the dice?, *Hydrological*
794 *Processes*, n/a-n/a, 10.1002/hyp.7574, 2009.

795 Boral, S., and Sen, I. S.: Tracing ‘Third Pole’ ice meltwater contribution to the Himalayan rivers
796 using oxygen and hydrogen isotopes, *Geochemical Perspectives Letters*, 48-53,
797 10.7185/geochemlet.2013, 2020.

798 Bowen, G. J., Cai, Z., Fiorella, R. P., and Putman, A. L.: Isotopes in the Water Cycle: Regional-
799 to Global-Scale Patterns and Applications, in: *Annual Review Of Earth And Planetary*
800 *Sciences*, Vol 47, edited by: Jeanloz, R., and Freeman, K. H., *Annual Review of Earth and*
801 *Planetary Sciences*, 453+, 2019.

802 Capell, R., Tetzlaff, D., and Soulsby, C.: Can time domain and source area tracers reduce
803 uncertainty in rainfall - runoff models in larger heterogeneous catchments?, *Water*
804 *Resources Research*, 48, 10.1029/2011wr011543, 2012.

805 Chen, X., Long, D., Hong, Y., Zeng, C., and Yan, D.: Improved modeling of snow and glacier
806 melting by a progressive two-stage calibration strategy with GRACE and multisource data:
807 How snow and glacier meltwater contributes to the runoff of the Upper Brahmaputra River
808 basin?, *Water Resources Research*, 53, 2431-2466, 10.1002/2016wr019656, 2017.

809 Chen, X., Long, D., Liang, S., He, L., Zeng, C., Hao, X., and Hong, Y.: Developing a composite
810 daily snow cover extent record over the Tibetan Plateau from 1981 to 2016 using
811 multisource data, *Remote Sen. Environ.*, 215, 284–299,
812 <https://doi.org/10.1016/j.rse.2018.06.021>, 2018.

813 Delavau, C. J., Stadnyk, T., and Holmes, T.: Examining the impacts of precipitation isotope
814 input on distributed, tracer-aided hydrological modelling, *Hydrology and Earth System*
815 *Sciences*, 21, 2595-2614, 10.5194/hess-21-2595-2017, 2017.

816 Didan, K.: MOD13A3 MODIS/Terra vegetation Indices Monthly L3 Global 1km SIN Grid
817 V006, NASA EOSDIS Land Processes DAAC [data set],
818 <https://doi.org/10.5067/MODIS/MOD13A3.006>, 2015.

819 Dong, G., Weng, B., Chen, J., Yan, D., and Wang, H.: Variation characteristics of stable isotopes
820 in water along main stream of Naqu River in source area of Nujiang River, *Water*
821 *Resources and Hydropower Engineering*, 49, 108-114, 2018.

822 Duethmann, D., Bolch, T., Farinotti, D., Kriegel, D., Vorogushyn, S., Merz, B., Pieczonka, T.,
823 Jiang, T., Su, B., and Guentner, A.: Attribution of streamflow trends in snow and glacier
824 melt-dominated catchments of the Tarim River, Central Asia, *Water Resources Research*,
825 51, 4727-4750, 10.1002/2014wr016716, 2015.

826 Dunn, S. M., McDonnell, J. J., and Vaché, K. B.: Factors influencing the residence time of
827 catchment waters: A virtual experiment approach, *Water Resources Research*, 43,

828 10.1029/2006wr005393, 2007.

829 Eriksson, D., Bindel, D., and Shoemaker, C.: Dme65/Pysot: V0.1.35, Zenodo [code],
830 <https://doi.org/10.5281/zenodo.569554>, 2017.

831 Gao J., Tian L., and Liu, Y.: Oxygen isotope variation in the water cycle of the Yamzho Lake
832 Basin in southern Tibetan Plateau, *Chinese Sci. Bull.*, 54, 2758–2765, 2009.

833 Gupta, H. V., Wagener, T., and Liu, Y.: Reconciling theory with observations: elements of a
834 diagnostic approach to model evaluation, *Hydrological Processes*, 22, 3802-3813,
835 10.1002/hyp.6989, 2008.

836 He, Y.: Pan-TPE soil map based on Harmonized World Soil Database (V1.2), National Tibetan
837 Plateau Data Center [data set], [https://data.tpdc.ac.cn/zh-hans/data/3519536a-d1e7-4ba1-](https://data.tpdc.ac.cn/zh-hans/data/3519536a-d1e7-4ba1-8481-6a0b56637baf?q=HWSO)
838 [8481-6a0b56637baf?q=HWSO](https://data.tpdc.ac.cn/zh-hans/data/3519536a-d1e7-4ba1-8481-6a0b56637baf?q=HWSO), 2019

839 He, Z. H., Tian, F. Q., Gupta, H. V., Hu, H. C., and Hu, H. P.: Diagnostic calibration of a
840 hydrological model in a mountain area by hydrograph partitioning, *Hydrology and Earth
841 System Sciences*, 19, 1807-1826, 10.5194/hess-19-1807-2015, 2015.

842 He, Z., Unger-Shayesteh, K., Vorogushyn, S., Weise, S. M., Kalashnikova, O., Gafurov, A.,
843 Duethmann, D., Barandun, M., and Merz, B.: Constraining hydrological model parameters
844 using water isotopic compositions in a glacierized basin, Central Asia, *Journal of
845 Hydrology*, 571, 332-348, 10.1016/j.jhydrol.2019.01.048, 2019.

846 He, Z., Unger-Shayesteh, K., Vorogushyn, S., Weise, S. M., Duethmann, D., Kalashnikova, O.,
847 Gafurov, A., and Merz, B.: Comparing Bayesian and traditional end-member mixing
848 approaches for hydrograph separation in a glacierized basin, *Hydrology and Earth System
849 Sciences*, 24, 3289-3309, 10.5194/hess-24-3289-2020, 2020.

850 He, Z., Duethmann, D., and Tian, F.: A meta-analysis based review of quantifying the
851 contributions of runoff components to streamflow in glacierized basins, *Journal of
852 Hydrology*, 603, 126890, 10.1016/j.jhydrol.2021.126890, 2021.

853 Hindshaw, R. S., Tipper, E. T., Reynolds, B. C., Lemarchand, E., Wiederhold, J. G., Magnusson,
854 J., Bernasconi, S. M., Kretzschmar, R., and Bourdon, B.: Hydrological control of stream
855 water chemistry in a glacial catchment (Damma Glacier, Switzerland), *Chemical Geology*,
856 285, 215-230, 10.1016/j.chemgeo.2011.04.012, 2011.

857 Immerzeel, W. W., van Beek, L. P. H., and Bierkens, M. F. P.: Climate Change Will Affect the
858 Asian Water Towers, *Science*, 328, 1382-1385, 10.1126/science.1183188, 2010.

859 Jeelani, G., Shah, R. A., Jacob, N., and Deshpande, R. D.: Estimation of snow and glacier melt
860 contribution to Liddar stream in a mountainous catchment, western Himalaya: an isotopic
861 approach, *Isotopes in environmental and health studies*, 53, 18-35,
862 10.1080/10256016.2016.1186671, 2017.

863 Kendall, C., and Coplen, T. B.: Distribution of oxygen-18 and deuterium in river waters across
864 the United States, *Hydrological Processes*, 15, 1363-1393, 10.1002/hyp.217, 2001.

865 Klaus, J., and McDonnell, J. J.: Hydrograph separation using stable isotopes: Review and
866 evaluation, *Journal of Hydrology*, 505, 47-64, 10.1016/j.jhydrol.2013.09.006, 2013.

867 Knapp, J. L. A., Neal, C., Schlumpf, A., Neal, M., and Kirchner, J. W.: New water fractions and
868 transit time distributions at Plynlimon, Wales, estimated from stable water isotopes in
869 precipitation and streamflow, *Hydrology and Earth System Sciences*, 23, 4367-4388,
870 10.5194/hess-23-4367-2019, 2019.

871 Kong, Y., Wang, K., Pu, T., and Shi, X.: Nonmonsoon Precipitation Dominates Groundwater
872 Recharge Beneath a Monsoon-Affected Glacier in Tibetan Plateau, *Journal of Geophysical
873 Research: Atmospheres*, 124, 10913-10930, 10.1029/2019jd030492, 2019.

874 Laudon, H., Taberman, I., Ågren, A., Futter, M., Ottosson-Löfvenius, M., and Bishop, K.: The
875 Krycklan Catchment Study-A flagship infrastructure for hydrology, biogeochemistry, and
876 climate research in the boreal landscape, *Water Resources Research*, 49, 7154-7158,
877 10.1002/wrcr.20520, 2013.

878 Li, Z.-J., Li, Z.-X., Song, L.-L., Gui, J., Xue, J., Zhang, B. J., and Gao, W. D.: Hydrological
879 and runoff formation processes based on isotope tracing during ablation period in the
880 source regions of Yangtze River, *Hydrology and Earth System Sciences*, 24, 4169-4187,
881 10.5194/hess-24-4169-2020, 2020.

882 Li, Z., Feng, Q., Li, Z., Yuan, R., Gui, J., and Lv, Y.: Climate background, fact and hydrological
883 effect of multiphase water transformation in cold regions of the western china: a review,
884 *EARTH SCIENCE REVIEWS*, 190, 33-57,
885 <https://doi.org/10.1016/j.earscirev.2018.12.004>, 2019.

886 Liu, S.: The second glacier inventory dataset of China (version 1.0) (2006–2011), National
887 Tibetan Plateau Data Center [data set], <https://doi.org/10.3972/glacier.001.2013.db>, 2012.

888 Liu, Z., Tian, L., Yao, T., Gong, T., Yin, C., and Yu, W.: Temporal and spatial variations of delta
889 O-18 in precipitation of the Yarlung Zangbo River Basin, *J. Geogr. Sci.*, 17, 317–326,
890 <https://doi.org/10.1007/s11442-007-0317-1>, 2007.

891 [Lone, A., Jeelani, G., Deshpande, R. D., and Padhya, V.: Estimating the sources of stream water
892 in snow dominated catchments of western Himalayas, *Advances in Water Resources*, 155,
893 \[10.1016/j.advwatres.2021.103995\]\(https://doi.org/10.1016/j.advwatres.2021.103995\), 2021.](#)

894 Lutz, A. F., Immerzeel, W. W., Shrestha, A. B., and Bierkens, M. F. P.: Consistent increase in
895 High Asia's runoff due to increasing glacier melt and precipitation, *Nature Climate Change*,
896 4, 587-592, 10.1038/nclimate2237, 2014.

897 McGuire, K. J., and McDonnell, J. J.: A review and evaluation of catchment transit time
898 modeling, *Journal of Hydrology*, 330, 543-563, 10.1016/j.jhydrol.2006.04.020, 2006.

899 McGuire, K. J., Weiler, M., and McDonnell, J. J.: Integrating tracer experiments with modeling
900 to assess runoff processes and water transit times, *Advances in Water Resources*, 30, 824-
901 837, 10.1016/j.advwatres.2006.07.004, 2007.

902 Myneni, R., Knyazikhin, Y., and Park, T.: MOD15A2H MODIS/Terra Leaf Area Index/FPAR
903 8-Day L4 Global 500m SIN Grid V006, NASA EOSDIS Land Processes DAAC [data set],
904 <https://doi.org/10.5067/MODIS/MOD15A2H.006>, 2015.

905 Nan, Y., Tian, F., Hu, H., Wang, L., and Zhao, S.: Stable Isotope Composition of River Waters
906 across the World, *Water*, 11, 1760, 10.3390/w11091760, 2019.

907 Nan, Y., He, Z., Tian, F., Wei, Z., and Tian, L.: Can we use precipitation isotope outputs of
908 isotopic general circulation models to improve hydrological modeling in large
909 mountainous catchments on the Tibetan Plateau?, *Hydrology and Earth System Sciences*,
910 25, 6151-6172, 10.5194/hess-25-6151-2021, 2021b.

911 Nan, Y., Tian, L., He, Z., Tian, F., and Shao, L.: The value of water isotope data on improving
912 process understanding in a glacierized catchment on the Tibetan Plateau, *Hydrology and
913 Earth System Sciences*, 25, 3653-3673, 10.5194/hess-25-3653-2021, 2021a.

914 Niinikoski, P. I. A., Hendriksson, N. M., and Karhu, J. A.: Using stable isotopes to resolve
915 transit times and travel routes of river water: a case study from southern Finland, *Isotopes
916 in environmental and health studies*, 52, 380-392, 10.1080/10256016.2015.1107553, 2016.

917 Ohlanders, N., Rodriguez, M., and McPhee, J.: Stable water isotope variation in a Central
918 Andean watershed dominated by glacier and snowmelt, *Hydrology and Earth System
919 Sciences*, 17, 1035-1050, 10.5194/hess-17-1035-2013, 2013.

920 Pomeroy, J. W., Gray, D. M., Brown, T., Hedstrom, N. R., Quinton, W. L., Granger, R. J., and
921 Carey, S. K.: The cold regions hydrological model: a platform for basing process
922 representation and model structure on physical evidence, *Hydrological Processes*, 21,
923 2650-2667, 10.1002/hyp.6787, 2007.

924 [Pu, T., Wang, K., Kong, Y. L., Shi, X. Y., Kang, S. C., Huang, Y. H., He, Y. Q., Wang, S. J., Lee,
925 J., and Cuntz, M.: Observing and Modeling the Isotopic Evolution of Snow Meltwater on
926 the Southeastern Tibetan Plateau, *Water Resources Research*, 56, 10.1029/2019wr026423,
927 2020.](#)

928 Rai, S. P., Singh, D., Jacob, N., Rawat, Y. S., Arora, M., and BhishmKumar: Identifying
929 contribution of snowmelt and glacier melt to the Bhagirathi River (Upper Ganga) near
930 snout of the Gangotri Glacier using environmental isotopes, *Catena*, 173, 339-351,
931 10.1016/j.catena.2018.10.031, 2019.

932 Reggiani, P., Hassanizadeh, S. M., Sivapalan, M., and Gray, W. G.: A unifying framework for
933 watershed thermodynamics: constitutive relationships, *Advances In Water Resources*, 23,
934 15-39, 10.1016/s0309-1708(99)00005-6, 1999.

935 Son, K., and Sivapalan, M.: Improving model structure and reducing parameter uncertainty in
936 conceptual water balance models through the use of auxiliary data, *Water Resources
937 Research*, 43, 10.1029/2006wr005032, 2007.

938 Sprenger, M., Stumpp, C., Weiler, M., Aeschbach, W., Allen, S. T., Benettin, P., Dubbert, M.,

939 Hartmann, A., Hrachowitz, M., Kirchner, J. W., McDonnell, J. J., Orłowski, N., Penna, D.,
940 Pfahl, S., Rinderer, M., Rodriguez, N., Schmidt, M., and Werner, C.: The Demographics
941 of Water: A Review of Water Ages in the Critical Zone, *Reviews Of Geophysics*, 57, 800-
942 834, 10.1029/2018rg000633, 2019.

943 Stevenson, J. L., Birkel, C., Neill, A. J., Tetzlaff, D., and Soulsby, C.: Effects of streamflow
944 isotope sampling strategies on the calibration of a tracer-aided rainfall-runoff model,
945 *Hydrological Processes*, 35, 10.1002/hyp.14223, 2021.

946 Tan, H., Chen, X., Shi, D., Rao, W., Liu, J., Liu, J., Eastoe, C. J., and Wang, J.: Base flow in the
947 Yarlungzangbo River, Tibet, maintained by the isotopically-depleted precipitation and
948 groundwater discharge, *The Science of the total environment*, 759, 143510,
949 10.1016/j.scitotenv.2020.143510, 2021.

950 Tetzlaff, D., Birkel, C., Dick, J., Geris, J., and Soulsby, C.: Storage dynamics in
951 hydrogeological units control hillslope connectivity, runoff generation, and the evolution
952 of catchment transit time distributions, *Water Resour Res*, 50, 969-985,
953 10.1002/2013WR014147, 2014.

954 Tian, F., Hu, H., Lei, Z., and Sivapalan, M.: Extension of the Representative Elementary
955 Watershed approach for cold regions via explicit treatment of energy related processes,
956 *Hydrology And Earth System Sciences*, 10, 619-644, 10.5194/hess-10-619-2006, 2006.

957 Tian, F., Xu, R., Nan, Y., Li, K., and He, Z.: Quantification of runoff components in the Yarlung
958 Tsangpo River using a distributed hydrological model, *Advances in Water Science*, 31,
959 324-336, 2020.

960 Tong, R., Parajka, J., Salentinig, A., Pfeil, I., Komma, J., Széles, B., Kubáň, M., Valent, P.,
961 Vreugdenhil, M., Wagner, W., and Blöschl, G.: The value of ASCAT soil moisture and
962 MODIS snow cover data for calibrating a conceptual hydrologic model, *Hydrology and
963 Earth System Sciences*, 25, 1389-1410, 10.5194/hess-25-1389-2021, 2021.

964 Viviroli, D., Weingartner, R., and Messerli, B.: Assessing the hydrological significance of the
965 world's mountains, *Mountain Research And Development*, 23, 32-40, 10.1659/0276-
966 4741(2003)023[0032:athstot]2.0.co;2, 2003.

967 Wang, C., Dong, Z., Qin, X., Zhang, J., Du, W., and Wu, J.: Glacier meltwater runoff process
968 analysis using δD and $\delta^{18}O$ isotope and chemistry at the remote Laohugou glacier basin
969 in western Qilian Mountains, China, *Journal of Geographical Sciences*, 26, 722-734,
970 10.1007/s11442-016-1295-y, 2016.

971 Wang, Y., Wang, L., Zhou, J., Yao, T., Yang, W., Zhong, X., Liu, R., Hu, Z., Luo, L., Ye, Q.,
972 Chen, N., and Ding, H.: Vanishing Glaciers at Southeast Tibetan Plateau Have Not Offset
973 the Declining Runoff at Yarlung Zangbo, *Geophysical Research Letters*, 48,
974 10.1029/2021gl094651, 2021.

975 Wolfe, B. B., Karst-Riddoch, T. L., Hall, R. I., Edwards, T. W. D., English, M. C., Palmini, R.,

976 McGowan, S., Leavitt, P. R., and Vardy, S. R.: Classification of hydrological regimes of
977 northern floodplain basins (Peace–Athabasca Delta, Canada) from analysis of stable
978 isotopes ($\delta^{18}\text{O}$, $\delta^2\text{H}$) and water chemistry, *Hydrological Processes*, 21, 151-168,
979 10.1002/hyp.6229, 2007.

980 Xi, X.: A Review of Water Isotopes in Atmospheric General Circulation Models: Recent
981 Advances and Future Prospects, *International Journal of Atmospheric Sciences*, 2014, 1-
982 16, 10.1155/2014/250920, 2014.

983 Xia, X., Li, S., Wang, F., Zhang, S., Fang, Y., Li, J., Michalski, G., and Zhang, L.: Triple oxygen
984 isotopic evidence for atmospheric nitrate and its application in source identification for
985 river systems in the Qinghai-Tibetan Plateau, *The Science of the total environment*, 688,
986 270-280, 10.1016/j.scitotenv.2019.06.204, 2019.

987 Xu, R., Hu, H., Tian, F., Li, C., and Khan, M. Y. A.: Projected climate change impacts on future
988 streamflow of the Yarlung Tsangpo-Brahmaputra River, *Global and Planetary Change*, 175,
989 144-159, 10.1016/j.gloplacha.2019.01.012, 2019.

990 Yang, K. and He, J.: China meteorological forcing dataset (1979–2018), National Tibetan
991 Plateau Data Center [data set],
992 <https://doi.org/10.11888/AtmosphericPhysics.tpe.249369.file>, 2019.

993 Yao, T., Masson-Delmotte, V., Gao, J., Yu, W., Yang, X., Risi, C., Sturm, C., Werner, M., Zhao,
994 H., He, Y., Ren, W., Tian, L., Shi, C., and Hou, S.: A review of climatic controls on $\delta^{18}\text{O}$
995 in precipitation over the Tibetan Plateau: Observations and simulations, *Reviews of*
996 *Geophysics*, 51, 525-548, 10.1002/rog.20023, 2013.

997 Yde, J. C., Knudsen, N. T., Steffensen, J. P., Carrivick, J. L., Hasholt, B., Ingeman-Nielsen, T.,
998 Kronborg, C., Larsen, N. K., Mernild, S. H., Oerter, H., Roberts, D. H., and Russell, A. J.:
999 Stable oxygen isotope variability in two contrasting glacier river catchments in Greenland,
1000 *Hydrology and Earth System Sciences*, 20, 1197-1210, 10.5194/hess-20-1197-2016, 2016.

1001 Yong, B., Wang, C.-Y., Chen, J., Chen, J., Barry, D. A., Wang, T., and Li, L.: Missing water
1002 from the Qiangtang Basin on the Tibetan Plateau, *Geology*, 49, 867-872, 10.1130/g48561.1,
1003 2021.

1004 Yoshimura, K., Kanamitsu, M., Noone, D., and Oki, T.: Historical isotope simulation using
1005 Reanalysis atmospheric data, *Journal of Geophysical Research*, 113,
1006 10.1029/2008jd010074, 2008.

1007 Zhang, F., Zhang, H. B., Hagen, S. C., Ye, M., Wang, D. B., Gui, D. W., Zeng, C., Tian, L. D.,
1008 and Liu, J. S.: Snow cover and runoff modelling in a high mountain catchment with scarce
1009 data: effects of temperature and precipitation parameters, *Hydrol. Process.*, 29, 52–65,
1010 <https://doi.org/10.1002/hyp.10125>, 2015.

1011 Zhang, Z., Chen, X., Cheng, Q., and Soulsby, C.: Storage dynamics, hydrological connectivity
1012 and flux ages in a karst catchment: conceptual modelling using stable isotopes, *Hydrology*

1014

1015 **List of Tables**

1016

1017 **Table 1.** Summary of precipitation and stream water samples in the YTR and KR catchments.

Catchment (Station)	Year	Sampling period	Precipitation			Stream		
			Sample number	$\overline{\delta^{18}\text{O}}$ (‰)	Std (‰)	Sample number	$\overline{\delta^{18}\text{O}}$ (‰)	Std (‰)
YTR (Nuxia)	2005	14/Mar to 23/Oct	86	-10.33	7.18	34	-15.74	1.60
YTR (Yangcun)		17/Mar to 05/ Oct	59	-13.17	7.10	30	-16.57	1.69
YTR (Nugesha)		14/Mar to 22/ Oct	45	-14.29	7.99	25	-17.84	0.99
YTR (Lazi)		06/ Jun to 22/Sep	42	-17.41	5.75	22	-16.52	1.43
	2006	06/Apr to 11/Nov	24	-15.22	3.83	31	-17.35	1.68
	2007	23/Apr to 09/ Oct	39	-16.99	5.93	25	-17.30	1.01
KR (Wengguo)	2010	05/May to 18/ Oct	63	-19.25	5.03	23	-17.44	1.29
	2011	28/Mar to 06/Nov	69	-13.99	5.90	32	-17.11	1.30
	2012	16/ Jun to 22/ Sep	42	-13.88	6.21	14	-17.01	0.60

1018

1019

1020 **Table 2.** Calibrated parameters of the THREW-T model

Symbol	Unit	Physical descriptions	Value range
nt	-	Manning roughness coefficient for hillslope	0-0.2
WM	cm	Tension water storage capacity, used in Xinanjiang model to calculate saturation area	0-10
B	-	Shape coefficient used in Xinanjiang model to calculate saturation area	0-1
KKA	-	Coefficient to calculate subsurface runoff in $Rg=KKD \cdot S \cdot K^S_s \cdot (y_s/Z)^{KKA}$, where S is the topographic slope, K^S_s is the saturated hydraulic conductivity, y_s is the depth of saturated groundwater, Z is the total soil depth	0-6
KKD	-	See description for KKA	0-0.5
T_0	°C	Temperature threshold above which snow and glacier melt	-5-5
DDF_N	mm/°C/day	Degree day factor for snowmelt	0-10
DDF_G	mm/°C/day	Degree day factor for glacier melt	0-10
$C1$	-	Coefficient to calculate the runoff concentration process using Muskingum method: $O_2=C_1 \cdot I_1+C_2 \cdot I_2+C_3 \cdot O_1+C_4 \cdot Q_{lat}$, where I_1 and O_1 is the inflow and outflow at prior step, I_2 and O_2 is the inflow and outflow at current step, Q_{lat} is lateral flow of the river channel, $C_3=I-C_1-C_2$, $C_4=C_1+C_2$	0-1
$C2$	-	See description for $C1$	0-1

1021

Table 3. Descriptions of water sampling scenarios in the three numerical experiments. $\delta^{18}\text{O}_{\text{GM}}$ is the assumed glacier meltwater isotope signature and $\overline{\delta^{18}\text{O}_{\text{PR}}}$ refers to the long term mean isotope signature of precipitation.

Experiment	Scenarios	Isotope data conditions
Benchmark model running in the YTR basin	BM_YTR	Using assumed glacier meltwater isotope as: $\delta^{18}\text{O}_{\text{GM}} = \overline{\delta^{18}\text{O}_{\text{PR}}} - 5\%$ Using IsoGSM outputs that were corrected by merged with sample measurements of precipitation isotope from four sampling sites Using all available stream water samples in the study period to calibrate the model
Benchmark model running in the KR catchment	BM_KR	Using all available stream water samples in the study period to calibrate the model
Experiment 1: Estimate of glacier meltwater isotope	G_Δ1	Assuming glacier meltwater isotope as: $\delta^{18}\text{O}_{\text{GM}} = \overline{\delta^{18}\text{O}_{\text{PR}}} - 1\%$
	G_Δ3	Assuming glacier meltwater isotope as: $\delta^{18}\text{O}_{\text{GM}} = \overline{\delta^{18}\text{O}_{\text{PR}}} - 3\%$
	G_Δ7	Assuming glacier meltwater isotope as: $\delta^{18}\text{O}_{\text{GM}} = \overline{\delta^{18}\text{O}_{\text{PR}}} - 7\%$
	G_Δ9	Assuming glacier meltwater isotope as: $\delta^{18}\text{O}_{\text{GM}} = \overline{\delta^{18}\text{O}_{\text{PR}}} - 9\%$
Experiment 2: Site sampling data of precipitation isotope	P_1station	Using IsoGSM outputs corrected by merged with measurements of precipitation isotope collected at one station (Nuxia) in YTR
	P_2stationNY	Using IsoGSM outputs corrected by merged with measurements of precipitation isotope collected at two stations (Nuxia and Yangcun) in YTR
	P_2stationNL	Using IsoGSM outputs corrected by merged with measurements of precipitation isotope collected at two stations (Nuxia and Lazi) in YTR
Experiment 3: Stream water sampling strategy for model evaluation	RT_YTR_BM	Sampling strategy: time series sampling; Sampling timing: wet season; Sampling frequency: weekly; Duration of sampling period: 1 year (2005); Number of sampling site: 1 station (Nuxia)
	RT_YTR_WholeYear	Same to RT_YTR_BM, but with the sampling timing as the whole study years
	RT_YTR_Monthly	Same to RT_YTR_BM, but with the sampling frequency as monthly
	RT_YTR_2year	Same to RT_YTR_BM, but with the duration of sampling period as only 2 years (2005 and 2006)
	RT_YTR_3year	Same to RT_YTR_BM, but with the duration of sampling period as only 3 years (2005-2007)
	RT_YTR_2station	Same to RT_YTR_BM, but with the number of sampling site as 2 stations (Nuxia and Yangcun)
	RT_YTR_4station	Same to RT_YTR_BM, but with the number of sampling site as 4 stations (Nuxia, Yangcun, Nugesha and Lazi)
	RS_YTR_Main	Sampling strategy: spatially distributed sampling in a single field campaign; Location of sampling site: along the main stream
	RS_YTR_Tributary	Same to RS_YTR_Main, but using stream water samples from additional sites along the tributaries
	RT_KR_1year	Sampling strategy: time series sampling; Duration of sampling period: 1 year (2006)
RT_KR_2year	Same to RT_KR_1year, but with the duration of sampling period as 2 years (2006 and 2007)	
RT_KR_3year	Same to RT_KR_1year, but with the duration of sampling period as 3 years (2006-2007, 2010)	
RT_KR_4year	Same to RT_KR_1year, but with the duration of sampling period as 4 years (2006-2007, 2010-2011)	
RT_KR_5year	Same to RT_KR_1year, but with the duration of sampling period as 5 years (2006-2007, 2010-2012)	

1026 **Table 4.** Contributions (%) of runoff components in the YTR basin and KR catchment
 1027 estimated by different calibration variants in the benchmark scenario.

Runoff Component	YTR basin		KR catchment	
	Bi-objective calibration*	Tri-objective calibration	Bi-objective calibration	Tri-objective calibration
Rainfall	62.8 (± 6.5)	70.7 (± 2.5)	46.4 (± 5.0)	43.9 (± 1.4)
Snowmelt	10.8 (± 1.1)	12.2 (± 0.4)	22.6 (± 2.4)	21.4 (± 0.7)
Glacier melt	26.4 (± 7.5)	17.1 (± 2.9)	31.0 (± 7.4)	34.6 (± 2.0)
Surface runoff	52.1 (± 10.5)	44.7 (± 6.7)	62.0 (± 10.9)	75.1 (± 3.3)
Subsurface runoff	47.9 (± 10.5)	55.3 (± 6.7)	38.0 (± 10.5)	24.9 (± 3.3)

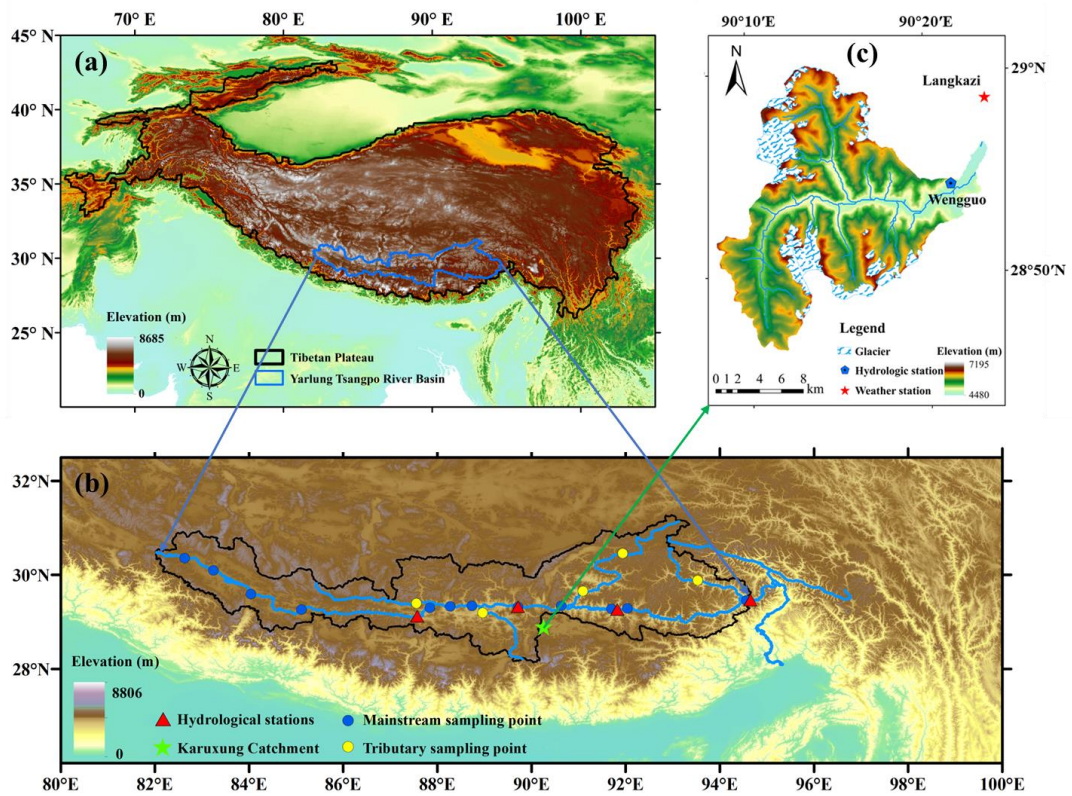
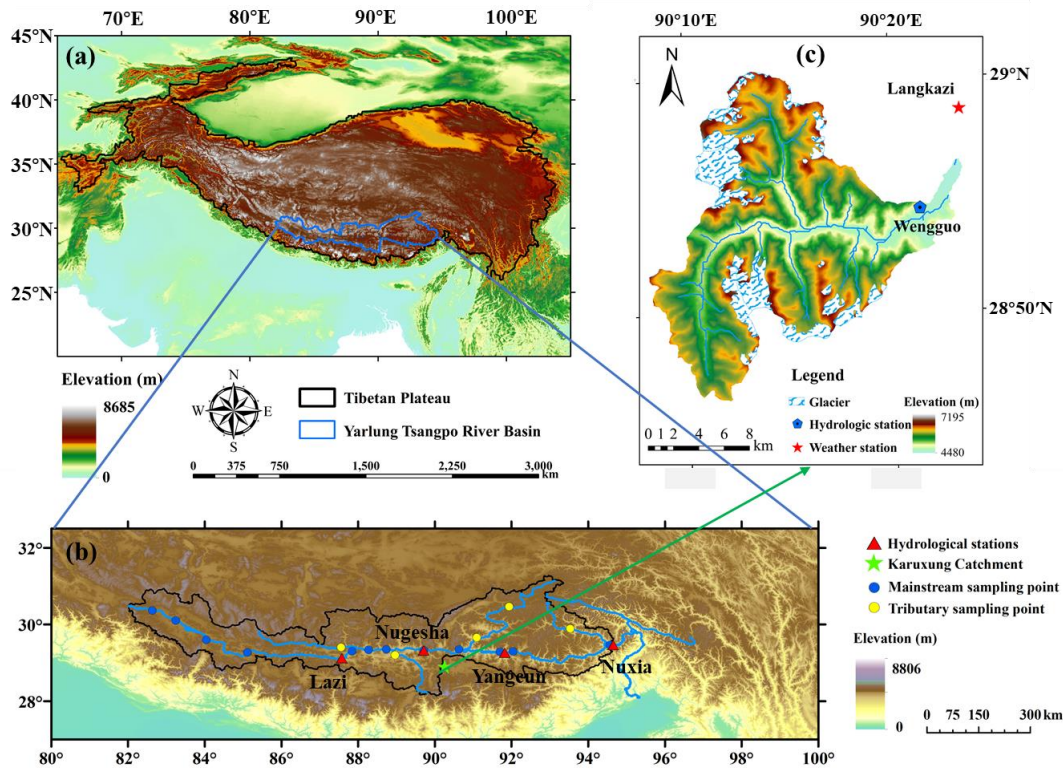
1028 *: Values in brackets refer to the standard deviation of the contribution of runoff component produced
 1029 by the behavioral parameter sets.

1030

1031 **Table 5.** Benchmark parameter set and corresponding model behavior that are used to produce
 1032 stream water $\delta^{18}\text{O}$ data for model calibration in experiment 3 in YTR basin.

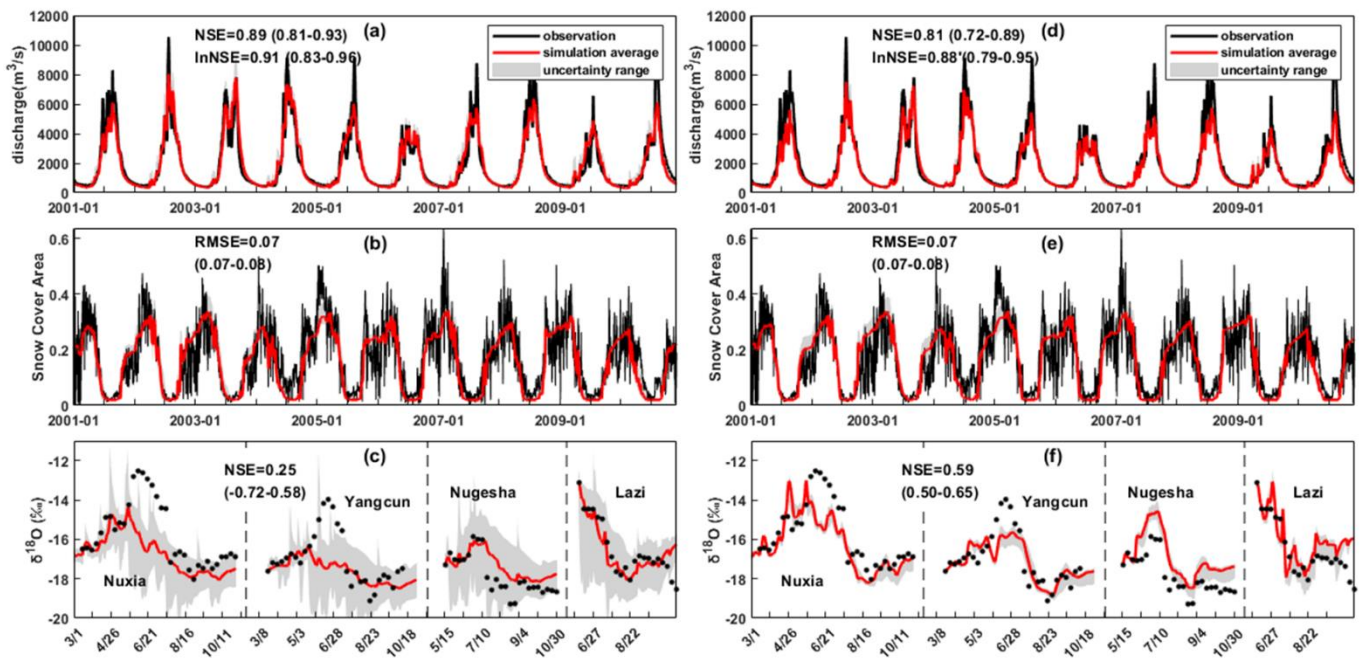
Parameter value		Model behavior	
<i>nt</i>	0.09	NSE _{dis} (Nuxia,calibration)	0.87
<i>WM</i>	0.92	NSE _{dis} (Nuxia,validation)	0.80
<i>B</i>	0.62	RMSE _{SCA} (calibration)	0.08
<i>KKA</i>	3.22	RMSE _{SCA} (validation)	0.12
<i>KKD</i>	0.14	NSE _{iso}	0.58
<i>T₀</i>	1.59	NSE _{dis} (Yangcun)	0.85
<i>DDF_N</i>	8.04	NSE _{dis} (Nugesha)	0.76
<i>DDF_G</i>	8.28	Contribution of rainfall	70%
<i>C1</i>	0.0004	Contribution of snowmelt	12%
<i>C2</i>	0.075	Contribution of glacier melt	18%
		Contribution of baseflow	56%

1033



1038 **Figure 1.** Locations and topography of the (a) Tibetan Plateau, (b) Yarlung Tsangpo river

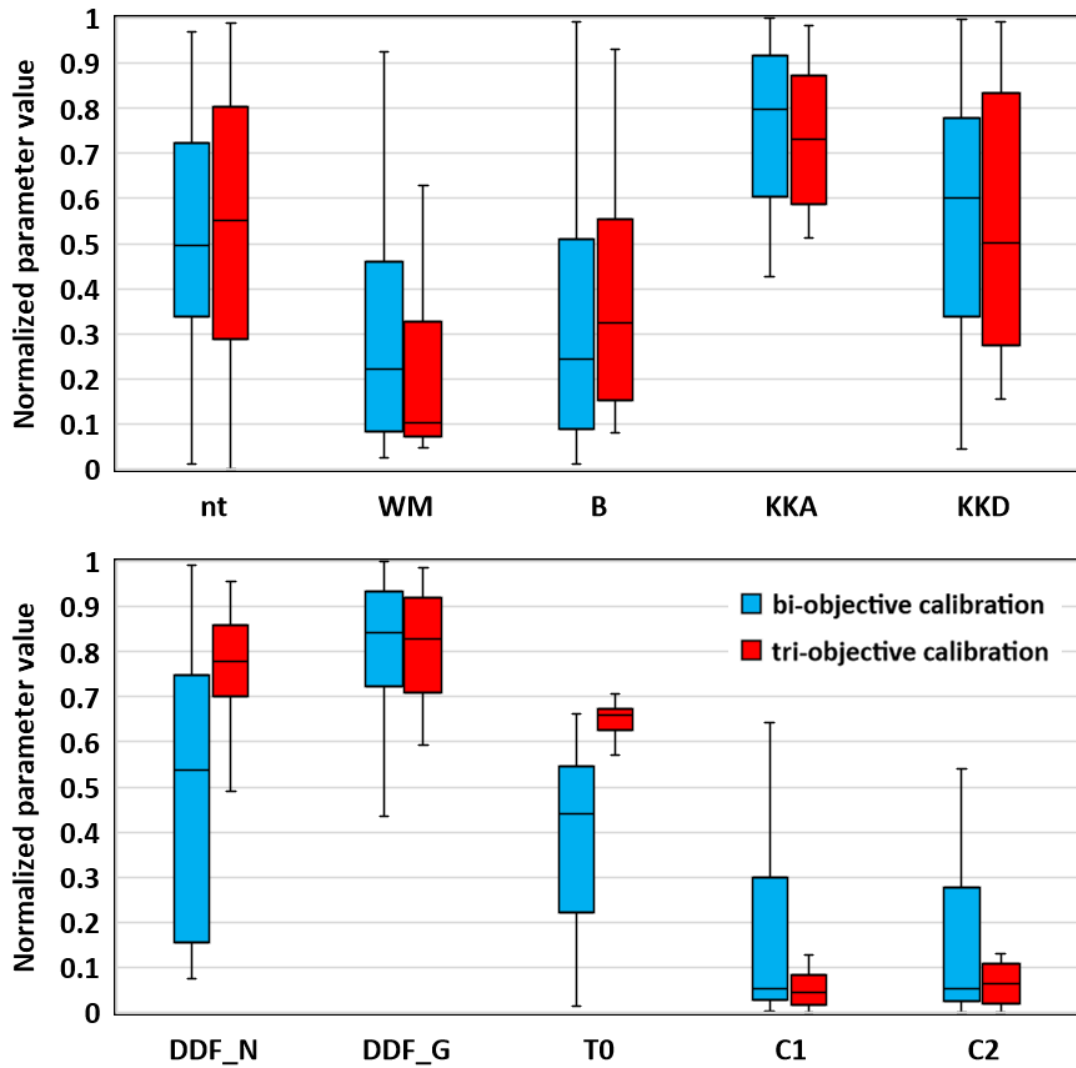
1039 basin and (c) Karuxung catchment. Triangles in figure b refer to hydrometric stations and
1040 sampling sites for precipitation and stream water isotope. Dots in figure b refer to assumed
1041 stream water sampling locations in RD_YTR scenarios.
1042



1043

1044 **Figure 2.** Uncertainty ranges and metrics values of the simulated discharge (Nuxia station),
 1045 SCA, and stream $\delta^{18}\text{O}$ (at four stations during 2005) in the YTR basin, that were produced by
 1046 the behavioral parameter sets of a bi-objective calibration (a-c) and a tri-objective (d-f)
 1047 calibration in the benchmark model running.

1048



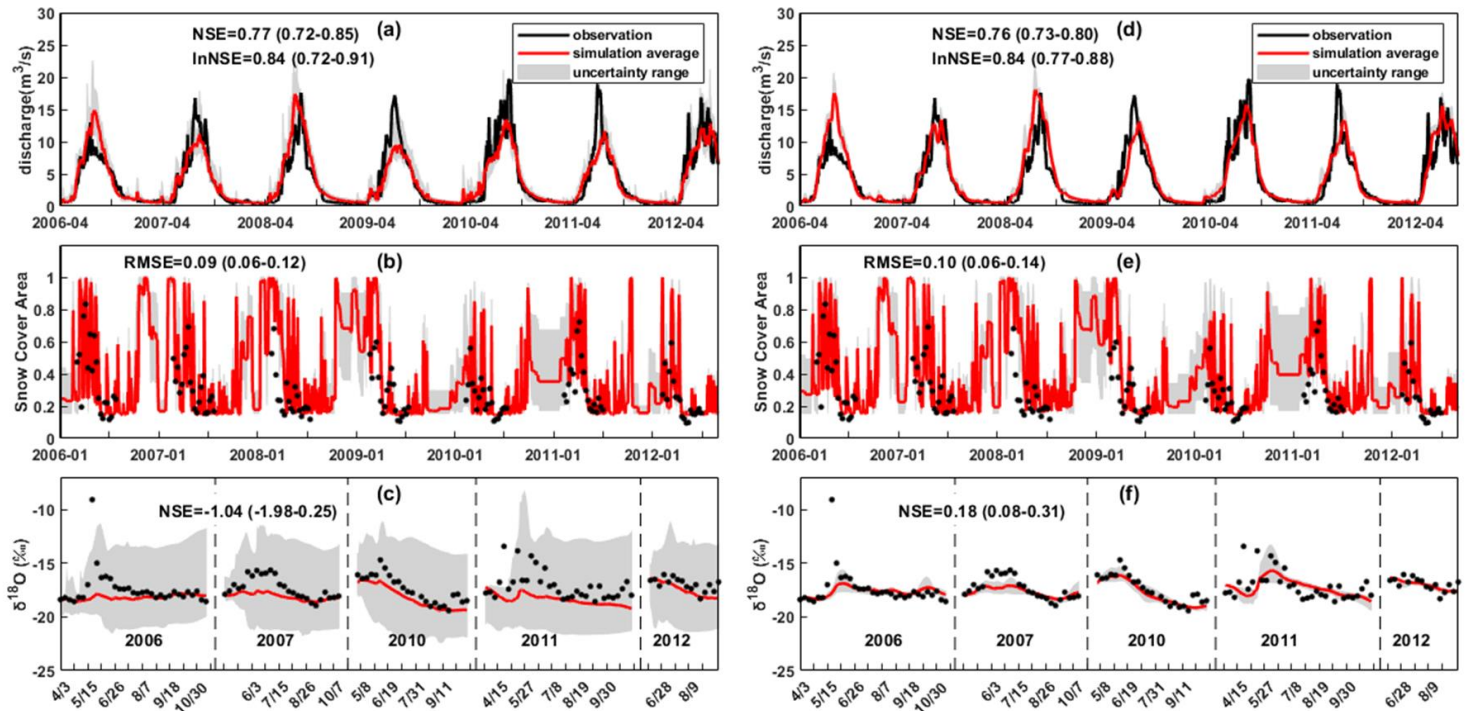
1049

1050

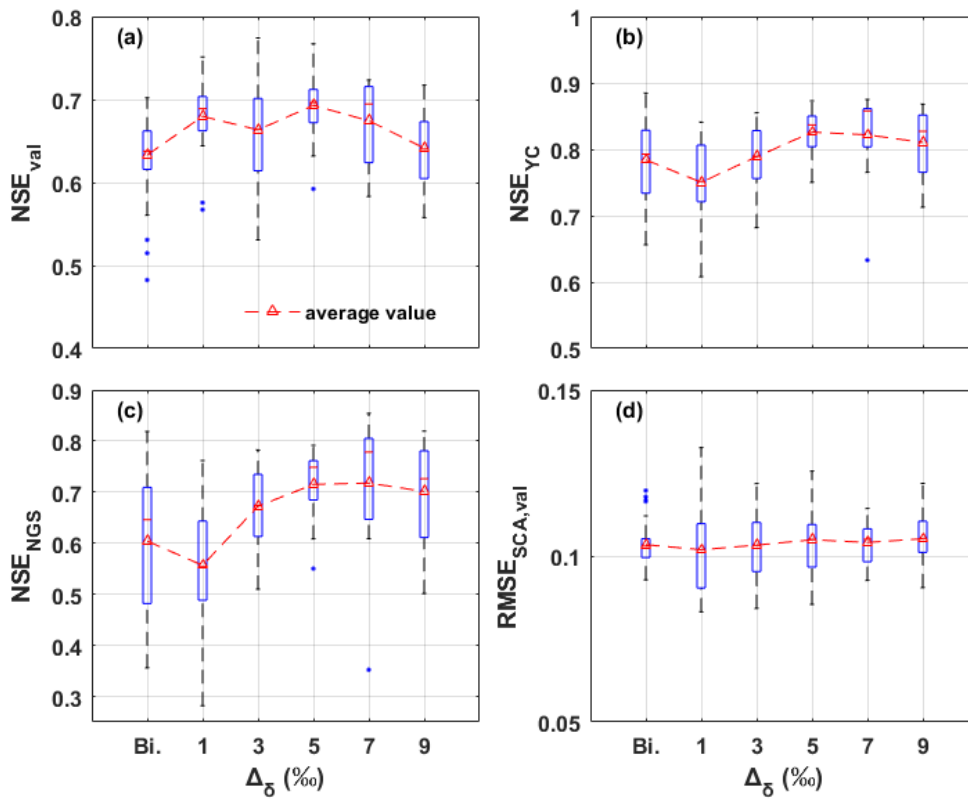
1051

1052

Figure 3. Uncertainties of behavioral parameter set obtained by bi- and tri-objective calibration methods for BM_YTR scenario in YTR basin.

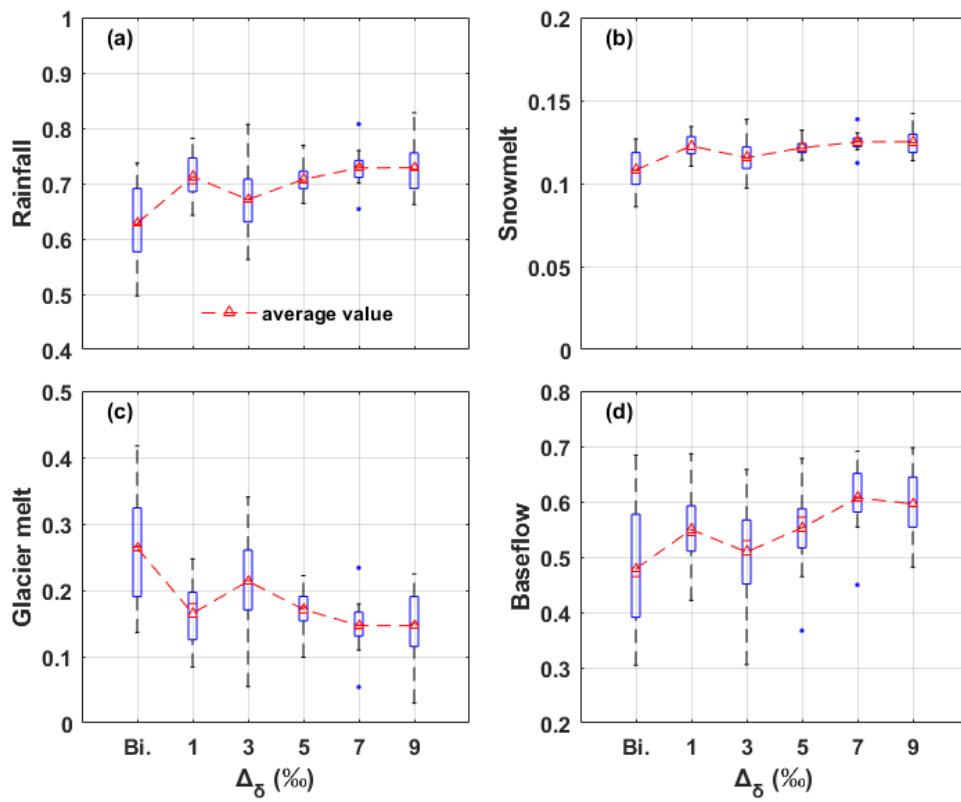


1055 **Figure 34.** Uncertainty ranges and metrics values of the simulated discharge, SCA, and
 1056 stream $\delta^{18}\text{O}$ in the KR catchment produced by the behavioral parameter sets of a bi-objective
 1057 calibration (a-c) and a tri-objective (d-f) calibration in the benchmark model running.

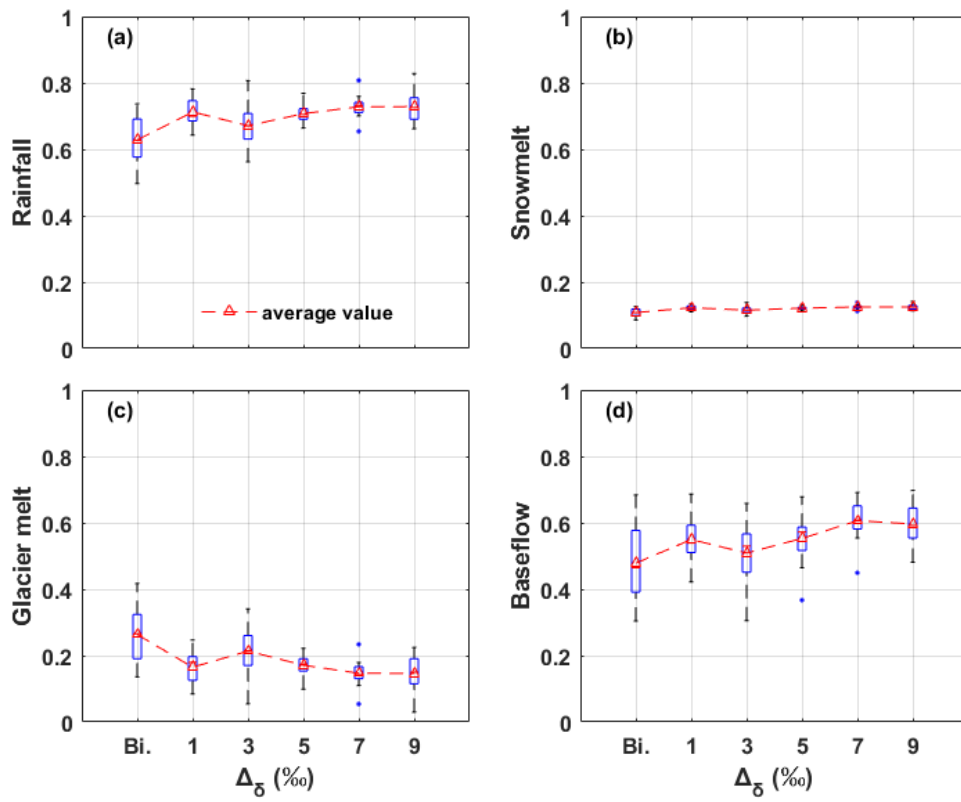


1059
 1060
 1061
 1062
 1063
 1064
 1065
 1066

Figure 45. Model performances in simulating discharge and SCA in the YTR basin in validation period/station produced by the behavioral parameter sets of scenarios using different glacier meltwater isotope inputs (experiment 1). Subplot (a) and (d) are the performances for Nuxia streamflow and SCA simulation in validation period, respectively. Subplot (b) and (c) are the performances for streamflow simulation in internal stations Yangcun and Nugesha, respectively.



1067



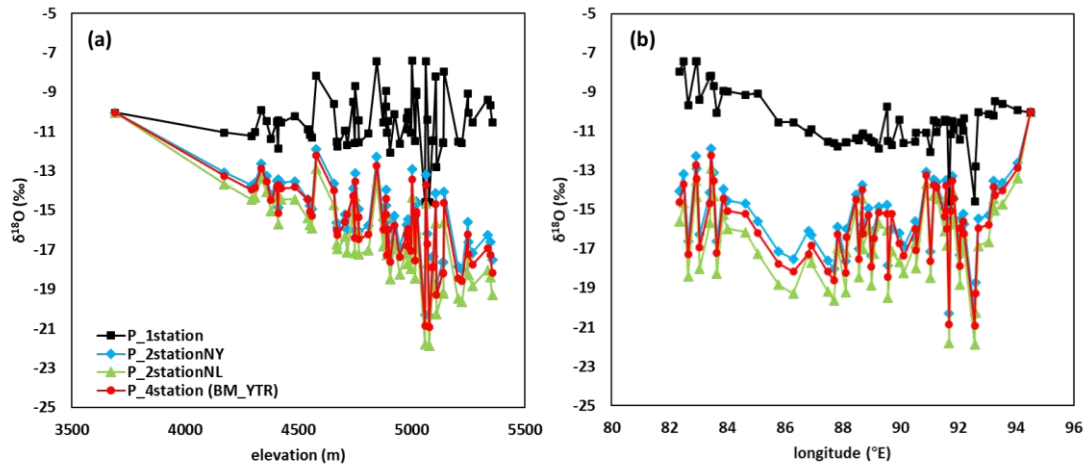
1068

1069

Figure 56. Runoff component contributions in the YTR basin estimated by the behavioral parameter sets of scenarios in experiment 1.

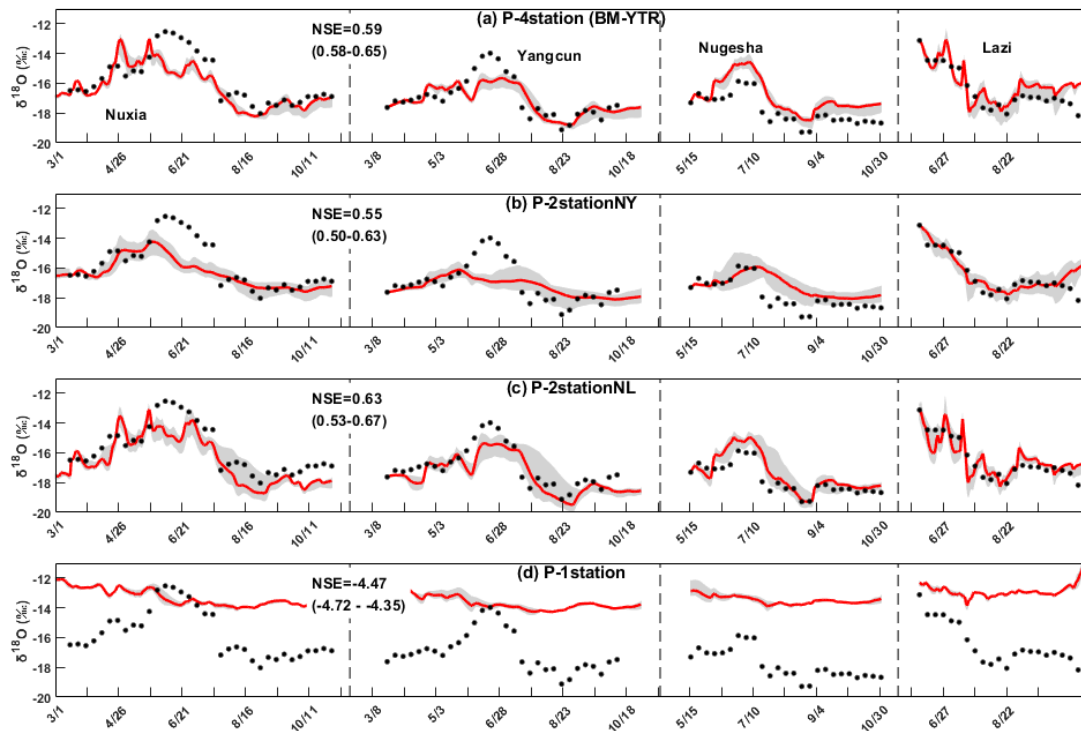
1070

1071



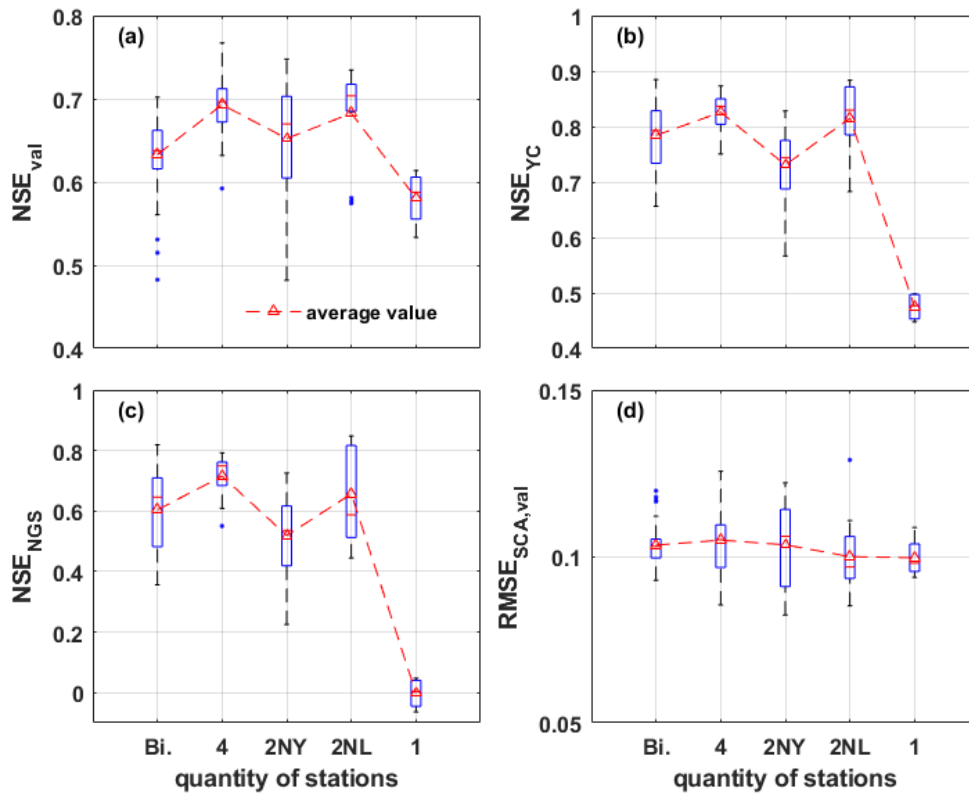
1072
 1073
 1074
 1075

Figure 7. Comparisons of weighted averages of precipitation $\delta^{18}\text{O}$ on 63 REWs in the YTR by elevation (a) and longitude (b) in each scenario of experiment 2.



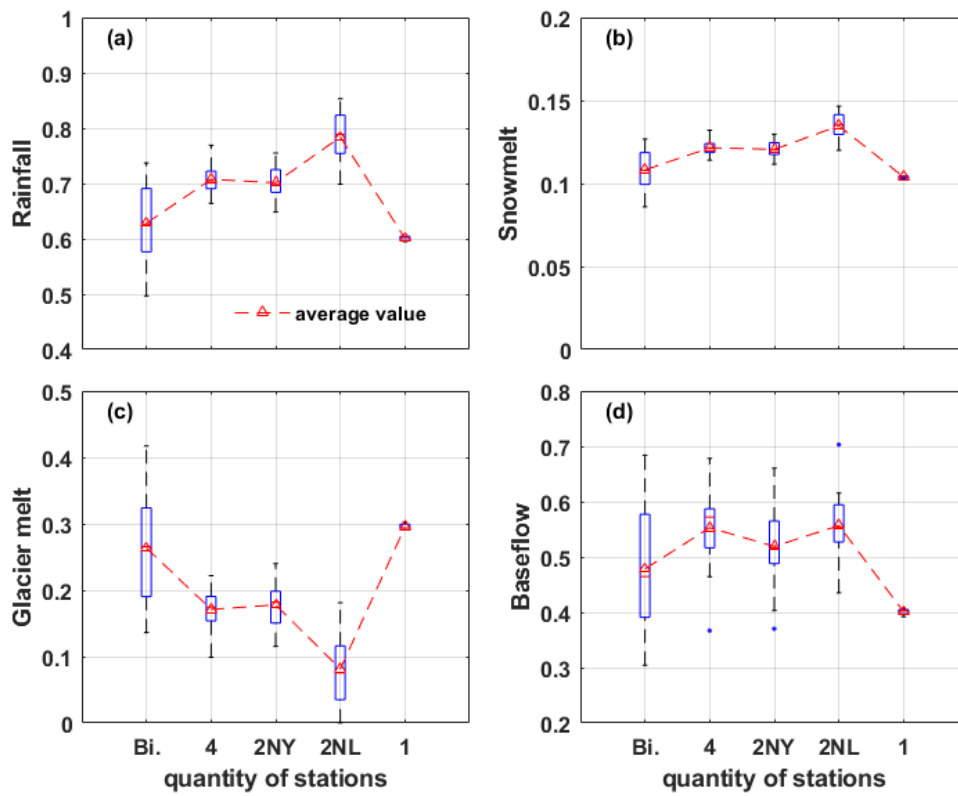
1076
 1077
 1078
 1079

Figure 8. Uncertainty ranges of stream water $\delta^{18}\text{O}$ simulations at four stations in 2005 produced by the behavioral parameter sets of each scenario in experiment 2.



1081

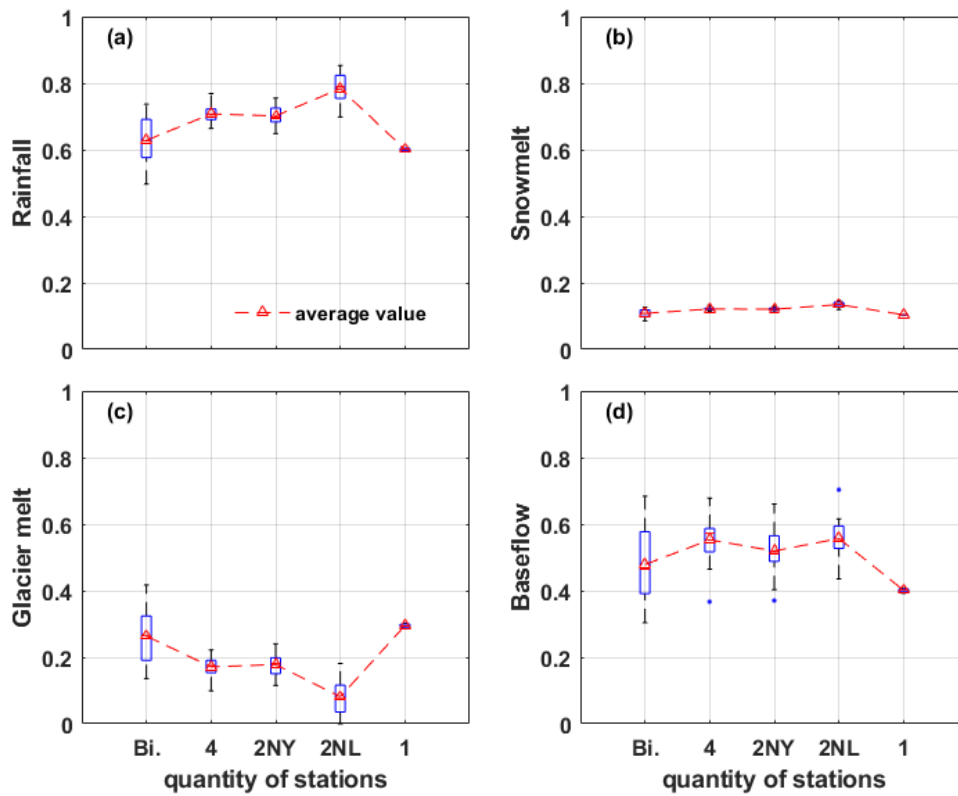
1082 **Figure 69.** Model performances in simulating discharge and SCA validation period/station in
 1083 YTR basin produced by the behavioral parameter sets of scenarios using precipitation isotope
 1084 measurements from different sampling sites (experiment 2). Subplot (a) and (d) are the
 1085 performances for Nuxia streamflow and SCA simulation in validation period, respectively.
 1086 Subplot (b) and (c) are the performances for streamflow simulation in internal stations
 1087 Yangcun and Nugesha, respectively.



1089

1090

⌈

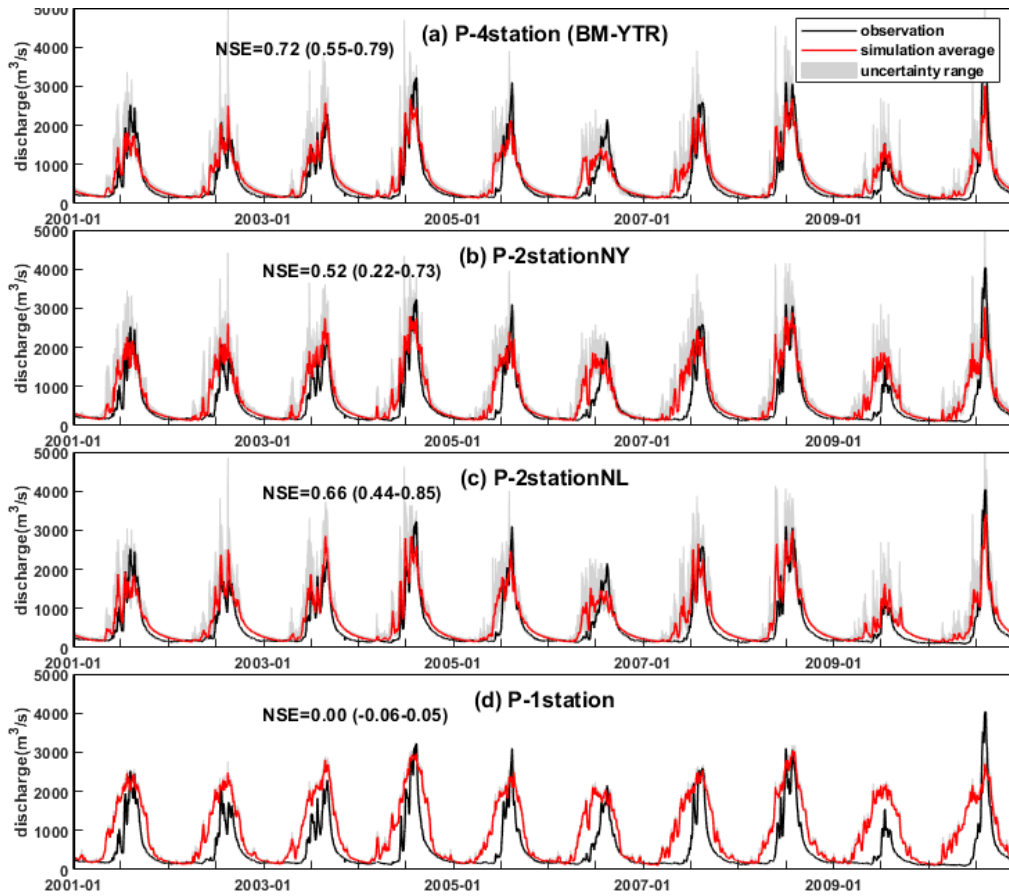


1091

1092

Figure 710. Runoff component contributions in the YTR basin estimated by the behavioral

1093 parameter sets of scenarios in experiment 2.
1094



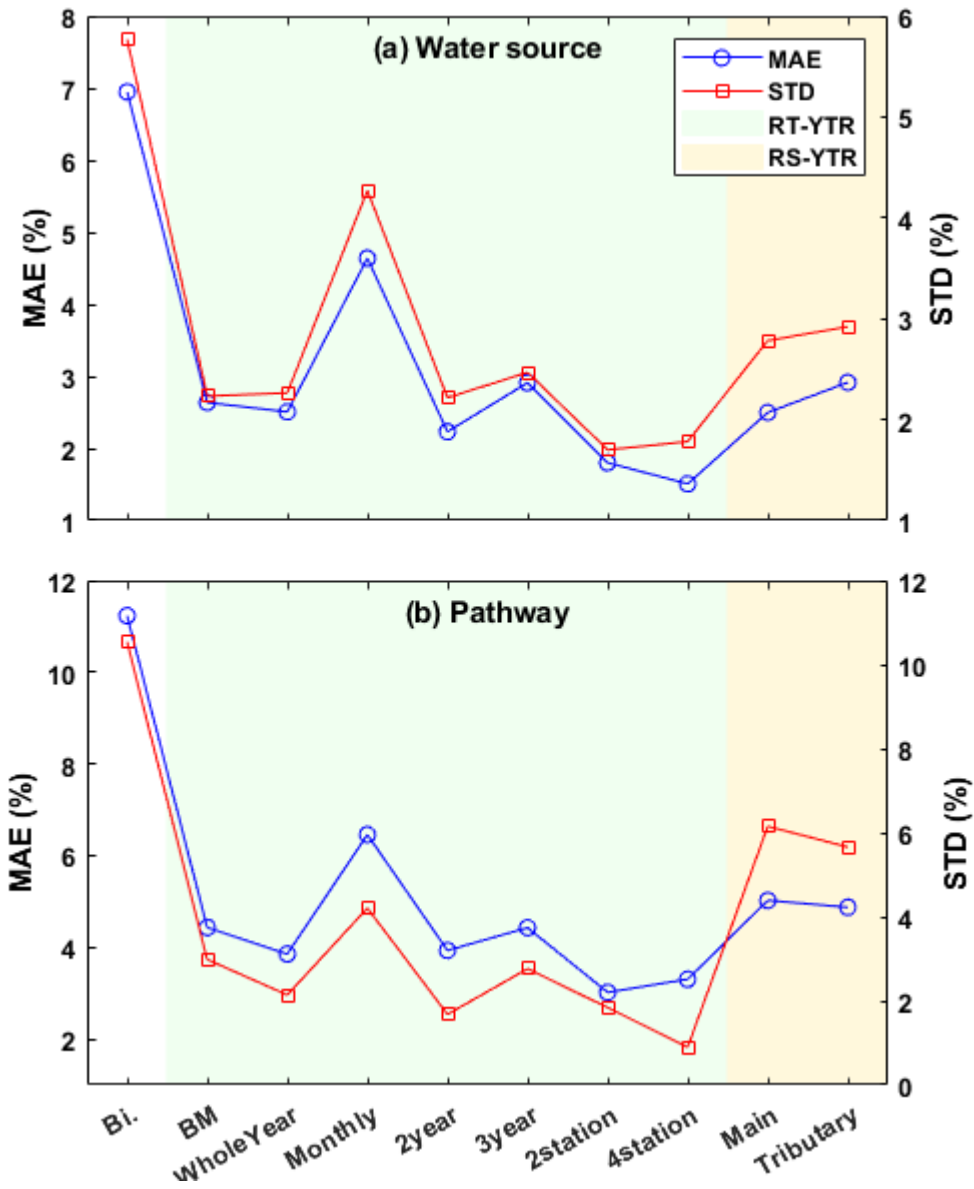
1095

1096

1097

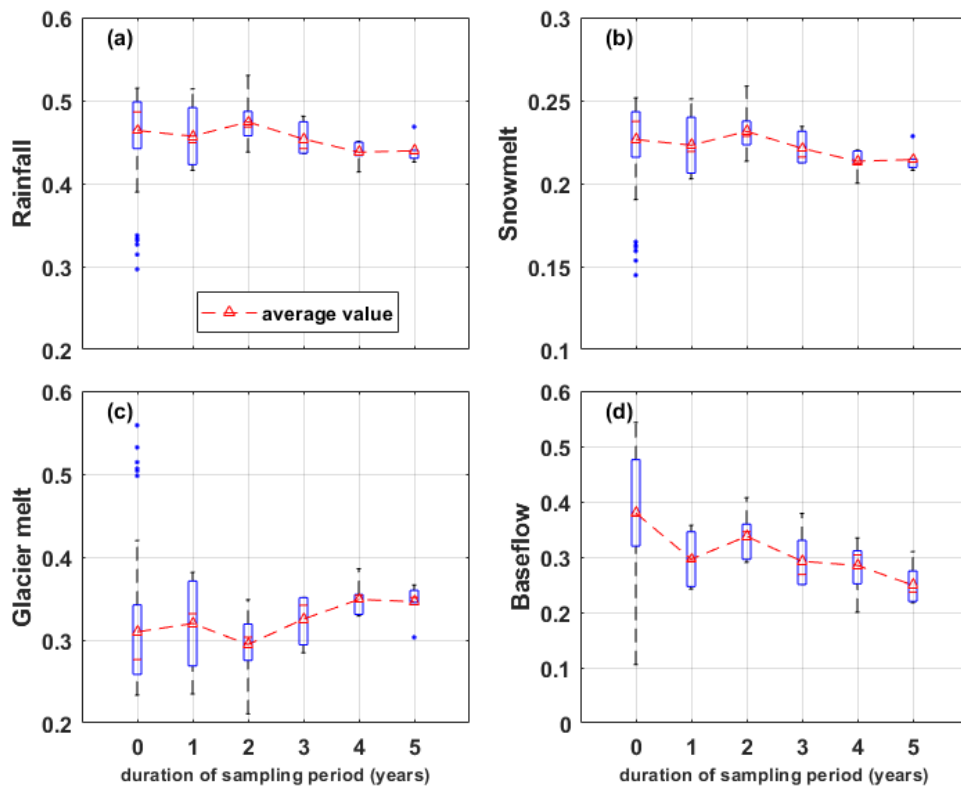
1098

Figure 811. Uncertainty range and metrics values of simulated discharge at Nugesha station produced by the behavioral parameter sets of each scenario in experiment 2.

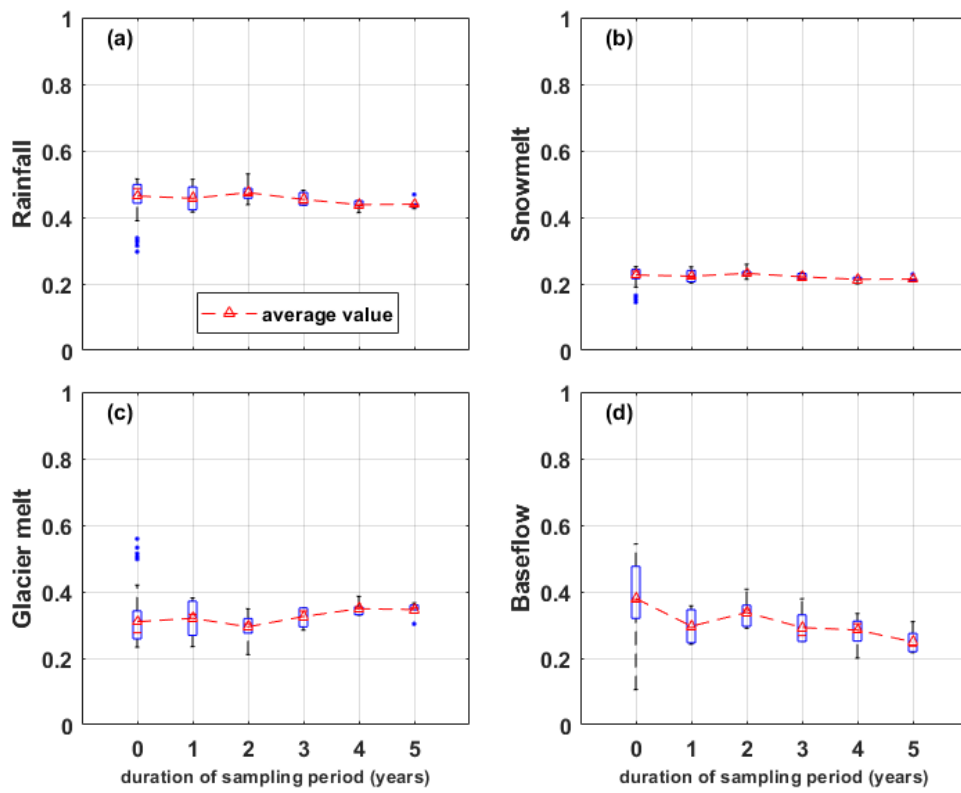


1099
 1100
 1101
 1102
 1103
 1104

Figure 912. Accuracy and uncertainty metrics of estimated CRCs in the YTR basin derived from the different stream water sampling strategies (experiment 3). (a) for CRCs quantified under the definition of water source and (b) for CRCs quantified under the definition of runoff pathway.



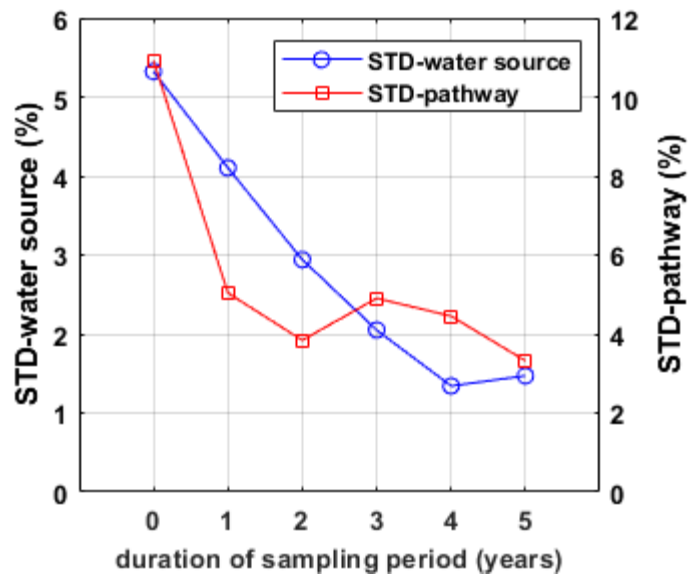
1105



1106

1107 **Figure 1013.** Uncertainties of the contributions of (a) rainfall, (b) snowmelt, (c) glacier melt
 1108 and (d) baseflow in the KR catchment, estimated by scenarios with different durations of

1109 sampling period (experiment 3).
1110



1111

1112 **Figure 11.14.** Uncertainty metrics of estimated CRCs in the KR catchment estimated by
 1113 scenarios with different durations of sampling period.

1114